AGU PUBLICATIONS

JGR

Journal of Geophysical Research: Atmospheres

RESEARCH ARTICLE
10.1002/2015JD024279

Special Section:
Deep Convective Clouds and Chemistry 2012 Studies (DC3)

This article is a companion to *Huntrieser et al.* [2016] doi:10.1002/2015JD024273.

On the origin of pronounced O_3 gradients in the thunderstorm outflow region during DC3

H. Huntrieser[1], M. Lichtenstern[1], M. Scheibe[1], H. Aufmhoff[1], H. Schlager[1], T. Pucik[1,2], A. Minikin[1], B. Weinzierl[1,3], K. Heimerl[1], D. Fütterer[1], B. Rappenglück[4], L. Ackermann[4], K. E. Pickering[5], K. A. Cummings[6], M. I. Biggerstaff[7], D. P. Betten[7], S. Honomichl[8], and M. C. Barth[8]

[1]Institut für Physik der Atmosphäre, Deutsches Zentrum für Luft- und Raumfahrt, Wessling, Germany, [2]Department of Geography, Masaryk University, Brno, Czech Republic, [3]Faculty of Physics, University of Vienna, Vienna, Austria, [4]Department of Earth and Atmospheric Sciences, University of Houston, Houston, Texas, USA, [5]Atmospheric Chemistry and Dynamics Laboratory, NASA Goddard Space Flight Center, Greenbelt, Maryland, USA, [6]Department of Atmospheric and Oceanic Science, University of Maryland, College Park, Maryland, USA, [7]School of Meteorology, University of Oklahoma, Norman, Oklahoma, USA, [8]NCAR, Boulder, Colorado, USA

Abstract Unique in situ measurements of CO, O_3, SO_2, CH_4, NO, NO_x, NO_y, VOC, CN, and rBC were carried out with the German Deutsches Zentrum für Luft- und Raumfahrt (DLR)-Falcon aircraft in the central U.S. thunderstorms during the Deep Convective Clouds and Chemistry experiment in summer 2012. Fresh and aged anvil outflow (9–12 km) from supercells, mesoscale convective systems, mesoscale convective complexes, and squall lines were probed over Oklahoma, Texas, Colorado, and Kansas. For three case studies (30 May and 8 and 12 June) a combination of trace species, radar, lightning, and satellite information, as well as model results, were used to analyze and design schematics of major trace gas transport pathways within and in the vicinity of the probed thunderstorms. The impact of thunderstorms on the O_3 composition in the upper troposphere/lower stratosphere (LS) region was analyzed. Overshooting cloud tops injected high amounts of biomass burning and lightning-produced NO_x emissions into the LS, in addition to low O_3 mixing ratios from the lower troposphere. As a dynamical response, O_3-rich air from the LS was transported downward into the anvil and also surrounded the outflow. The $\Delta O_3/\Delta CO$ ratio was determined in the anvil outflow region. A pronounced in-mixing of O_3-rich stratospheric air masses was observed in the outflow indicated by highly positive or even negative $\Delta O_3/\Delta CO$ ratios (+1.4 down to −3.9). Photochemical O_3 production ($\Delta O_3/\Delta CO = +0.1$) was found to be minor in the recently lofted pollution plumes. O_3 mixing ratios within the aged anvil outflow were mainly enhanced due to dynamical processes.

Key Points:
- Overshooting of the central U.S. severe thunderstorms probed in situ by aircraft
- $\Delta O_3/\Delta CO$ ratios were determined for fresh and aged (~12–24 h) anvil outflow
- O_3 enhanced (~20–50 nmol mol^{-1}) in the aged anvil outflow mainly due to dynamical processes

Correspondence to:
H. Huntrieser,
Heidi.Huntrieser@dlr.de

Citation:
Huntrieser, H., et al. (2016), On the origin of pronounced O_3 gradients in the thunderstorm outflow region during DC3, *J. Geophys. Res. Atmos., 121*, 6600–6637, doi:10.1002/2015JD024279.

Received 28 SEP 2015
Accepted 3 MAR 2016
Accepted article online 9 MAR 2016
Published online 11 JUN 2016

1. Introduction

Ozone (O_3) plays a key role for the chemical composition in the atmosphere and acts as a prominent greenhouse gas in the upper troposphere (UT) [*Myhre et al.*, 2013]. The main sources of tropospheric ozone are photochemical production and downward transport (entrainment) of O_3-rich air from the stratosphere [*Crutzen*, 1995; *Stevenson et al.*, 2006]. Emissions from natural and anthropogenic sources in the boundary layer (BL) (e.g., wildfires and fossil fuel combustion) are rich in O_3 precursors such as carbon monoxide (CO), methane (CH_4), and volatile organic compounds (VOCs) and can be uplifted to the UT by warm conveyor belts and/or deep convection [*Cooper et al.*, 2004]. In the UT, O_3 precursors are emitted from lightning-produced NO_x ($\triangleq NO + NO_2$) (LNO_x) and aircraft, where LNO_x (5 ± 3 Tg a^{-1}) is the most important natural O_3 precursor in the UT [*Schumann and Huntrieser*, 2007]. In the presence of hydrogen oxides ($HO_x = HO + HO_2$) and NO (also from anthropogenic sources) O_3 can be produced by photochemical oxidation of the precursors [*Crutzen*, 1970; *Fishman et al.*, 1979]. Due to the increasing lifetime of tropospheric NO_x with altitude (a few hours in the BL and ~2–3 days in the UT), it is possible to trace thunderstorm outflow ~1–2 days after the thunderclouds have dissipated [*Huntrieser et al.*, 2002].

Due to the large variety of the processes mentioned above, measurements inside and in the vicinity of thunderstorms have shown a wide spectrum of O_3 mixing ratios. Almost zero ozone has been measured in the convective outflow over remote unpolluted regions (e.g., tropical Pacific) because of direct upward transport of low O_3 mixing ratios from the marine BL [*Kley et al.*, 1996; *Folkins et al.*, 2002]. Elevated O_3 in the range of 100 ppbv (or nmol mol^{-1}) has been observed in the outflow of continental thunderstorms as a result of

convective transport of surface polluted air followed by downwind chemistry [*Pickering et al*., 1990, 1996]. Extreme O_3-rich transients of a few hundred up to ~2000 nmol mol^{-1} O_3 have been measured in humidified air masses affected by convection over tropical oceanic and rain forest areas possibly because of natural and artificial corona discharges [*Zahn et al*., 2002; *Ridley et al*., 2006; *Bozem et al*., 2014]; on the other hand, a stratospheric influence has been suggested [*Suhre et al*., 1997]. Further explanations for this wide O_3 range observed in fresh and aged anvil outflow are discussed below and in section 5. A method to distinguish the different processes impacting the O_3 composition is described next.

Ozone enhancements observed in the troposphere, whether photochemically produced or transported downward from the stratosphere, are generally distinguished by the sign of the O_3-CO correlation, as introduced by *Fishman and Seiler* [1983] for aircraft measurements. In the stratosphere, CO decreases with increasing O_3 mixing ratios. Negative O_3-CO regression slopes characterize the downward transport of stratospheric air masses into the troposphere. Positive slopes have been observed in aged lofted pollution and biomass burning (BB) plumes rich in CO and photochemically produced O_3, not only in the tropics but also at higher latitudes [*Parrish et al*., 1993; *Chin et al*., 1994; *Singh et al*., 2010; *Jaffe and Wigder*, 2012]. The linear regression slope of the O_3-CO correlation can also be expressed as $\Delta O_3/\Delta CO$ ratio in nmol mol^{-1}/nmol mol^{-1}. Up to now, not much is known about which of the above mentioned processes dominate the O_3 budget and the O_3-CO correlation within the anvil outflow from thunderstorms. *The main objective of the present study is to analyze processes affecting the O_3 composition in the UT/lower stratosphere (LS) region over the central United States (U.S.) during the Deep Convective Clouds and Chemistry (DC3) experiment*. More specifically, *Which $\Delta O_3/\Delta CO$ ratios were observed within and in the vicinity of the probed thunderstorms and how can they be explained?* The DC3 field experiment has been described in detail by *Barth et al*. [2015] and in HH2016 (which refers to *Huntrieser et al*. [2016]). In the present study details on DC3 are given later in this section and in section 2.

The major processes that may affect the O_3 composition in the thunderstorm outflow region and its range are briefly summarized next: (1) photochemical O_3 production by BB emissions, (2) photochemical O_3 production by LNO_x emissions, and (3) stratosphere-troposphere exchange.

1. *Photochemical O_3 production by BB (and mixed in anthropogenic) emissions*. In general, anthropogenic pollution sources were low in the DC3 thunderstorm inflow regions over the central U.S. [*Barth et al*., 2015; HH2016]. However, during DC3 some of the largest and *most destruc*tive wildfires in New Mexico and Colorado state's history were burning, which strongly influenced air quality in the DC3 thunderstorm inflow and outflow region, as described later (see section 3). In a review article by *Jaffe and Wigder* [2012], *the O_3-CO regression slope in air masses impacted by wildfires was given a range from −0.1 to +0.9*, however, most likely from nearly zero to +0.7, based on many single observations around the world. In boreal regions, O_3-CO ratios tend to be low (O_3 enhancement <5 nmol mol^{-1}), due to a low nitrogen content in boreal vegetation and low emission rates of urban pollution (O_3 precursors) [*Alvarado et al*., 2010; *Singh et al*., 2010]. Furthermore, the cooler temperature and lower insolation in these regions favor slow O_3 production rates. In the middle to upper troposphere (5–9 km) at high northern latitudes, *Singh et al*. [2010] reported a correlation ratio of $\Delta O_3/\Delta CO = +0.1$ in aged BB and urban plumes observed during Arctic Research of the Composition of the Troposphere from Aircraft and Satellites (ARCTAS). A tendency to higher correlation ratios (up to +0.5) has been observed in BB plumes mixed with heavier urban pollution over North America (NA) [*Hecobian et al*., 2011; *Wigder and Jaffe*, 2013]. In aged BB plumes affected by tropical deep convection, an O_3 formation rate of 7–8 nmol mol^{-1} d^{-1} has been calculated in case studies, and an O_3 enhancement in the range of 30 nmol mol^{-1} after 5 days transport has been observed [*Pickering et al*., 1996; *Thompson et al*., 1997]. Elevated $\Delta O_3/\Delta CO$ ratios, up to +0.8, have been observed in Asian pollution plumes transported in the UT to NA [*Price et al*., 2004; *Bertschi and Jaffe*, 2005; *Liang et al*., 2007]. Both strong photochemical production due to high pollution levels and mixing processes with stratospheric air masses along isentropic surfaces have been suggested as explanations for these high ratios. A number of observations have shown that the interweaving of stratospheric intrusions with pollution plumes may complicate the fine-scale $\Delta O_3/\Delta CO$ correlations [*Parrish et al*., 2000; *Nowak et al*., 2004; *Price et al*., 2004; *Liang et al*., 2007].
2. *Photochemical O_3 production by LNO_x*. In the literature a wide range of *convective ozone production enhancements ranging up to ~20 nmol mol^{-1} d^{-1}* have been published [*Morris et al*., 2010, Table 1; *Bozem et al*., 2014, Table 3]. However, ozone production rates as high as ~5 nmol mol^{-1} h^{-1}, as found in *Morris et al*. [2010] study, may be unrealistic. Model simulations indicate that most of the O_3 production

happens within the first 24 h after convection occurs [*Barth et al*., 2012]. In cases with higher production rates, the presence of anthropogenic pollution and BB emissions, in addition to LNO_x, seems to play an important role for the enhanced O_3 production in the convective outflow [*Real et al*., 2010]. Recently, the importance of isoprene (emitted from vegetation) for especially high O_3 production rates in modeled LNO_x plumes has been pointed out [*Apel et al*., 2012]. For a Stratospheric-Tropospheric Experiment: Radiation, Aerosols, and Ozone (STERAO-A) thunderstorm (central U.S.) and a European Lightning Nitrogen Oxides (EULINOX) thunderstorm (southern Germany), where mainly LNO_x played a role for the O_3 production, *DeCaria et al*. [2005] and *Ott et al*. [2007] calculated O_3 production rates on the order of ~5 and up to 13 nmol mol^{-1} d^{-1}, respectively. For a tropical thunderstorm over Suriname, *Bozem et al*. [2014] calculated a production rate of 5–11 nmol mol^{-1} O_3 per day based on HO_x measurements over the tropical rain forest. For two DC3 thunderstorms strongly impacted by BB emissions on 22 June 2012 box model calculations (initialized with measurements in the outflow) by *Apel et al*. [2015] predicted a production rate of 11 and 14 nmol mol^{-1} O_3, respectively, over a two-day period.

3. *Stratosphere-troposphere exchange*. Besides the strong influence of BB plumes on the thunderstorm environment during DC3, the interaction with O_3-rich air masses from the stratosphere was also prominent as already mentioned in HH2016. Evidence from aircraft and satellite observations of extratropical convection injecting BL air into the lowermost stratosphere (LMS), e.g., forming filaments 50–100 km in width and several 1000 km in length, has already been reported in previous studies [*Roach*, 1967; *Poulida et al*., 1996; *Fischer et al*., 2003; *Hegglin et al*., 2004; *Ray et al*., 2004; *Anderson et al*., 2012; *Homeyer et al*., 2014]. Besides the deep convective upward transport, traces of downward intrusions of O_3-rich air masses from the stratosphere into the anvil outflow region have been modeled in a number of studies [*Wang et al*., 1995; *Stenchikov et al*., 1996; *Tang and Prather*, 2010; *Homeyer et al*., 2011; *Tang et al*., 2011; *Frey et al*., 2015]. However, this process has infrequently been observed before the DC3 field experiment was conducted. Only a few observations are available [*Dickerson et al*., 1987; *Poulida et al*., 1996; *Winterrath et al*., 1999; *Dye et al*., 2000; *Hitchman et al*., 2004; *Homeyer et al*., 2011]. Different processes have been described in the literature causing a downward intrusion. *Boatman and Auer* [1983] and *Blyth et al*. [1988] introduced the so-called "cloud top entrainment" mechanism: O_3-rich air masses from above mixes into the upper tropospheric anvil outflow. A distinct rear inflow from the stratosphere was observed in a Mesoscale Convective System (MCS) by *Houze et al*. [1989] based on Doppler radar analyses. Recently, *Pan et al*. [2014] presented the first evidence in lidar images of a pronounced downward transport of O_3-rich stratospheric air masses wrapping around the anvil outflow of a MCS during DC3. Evidence of mixing between polluted convective outflow and stratospheric air in the UT during DC3 was recently also described by *Schroeder et al*. [2014].

As previously stated, the objective of the present study is to investigate if and how the above mentioned processes (1), (2), and (3) affected the O_3 composition in the thunderstorm outflow region during DC3. The airborne in situ thunderstorm observations presented throughout this paper will contribute to answer the following questions. *(1) Did deep convection during DC3 substantially impact the O_3 budget in the UT/LS region? (2) What processes, coinciding with DC3 deep convection, affect the O_3 budget over the central U.S.: chemical and/or dynamical processes? (3) Which of these processes dominate the O_3 budget in the fresh and aged (0–12/12–24 h) thunderstorm outflow during DC3?*

The DC3 field campaign was carried out from Kansas in May–June 2012. The general experimental setup is described by *Barth et al*. [2015]. An accompanying DC3 study is introduced in HH2016 where measurements with the German research aircraft of the Deutsches Zentrum für Luft- und Raumfahrt (DLR), a Falcon-20, and one joint flight with the two U.S. aircraft (NASA-DC8 and NSF/NCAR-Gulfstream-V (GV)) are presented. In HH2016 the primary objective is to give an overview of the Falcon measurements and to study emissions from wildfires and LNO_x within and in the vicinity of the fresh thunderstorm outflow. A secondary objective is to analyze the dynamics of a single storm system and its impact on the O_3 and aerosol composition in the UT/LS region. The analyses are based on vertical profiles of trace species and tracer-tracer correlations (CO-NO_x and O_3-NO). The stratosphere-troposphere exchange of O_3 and H_2O is touched upon; however, the exchange of O_3 is highlighted first in the present study.

Here we show detailed analyses based on three Falcon flights during DC3. During these flights the fresh and aged anvil outflow in supercells, Mesoscale Convective Complexes (MCCs), MCSs, and squall lines were

probed extensively with the Falcon up to 12 km altitude (for storm definitions see *Maddox* [1980], *Houze et al*. [1989], and *Houze* [2004]). A number of trace species, such as sulphur dioxide (SO_2), CO, O_3, CH_4, NO, NO_x, NO_y, VOCs, condensation nuclei (CN), and refractory black carbon (rBC), were measured in situ with the Falcon. On the basis of trace species time series and tracer-tracer correlations (O_3-CO) the impact on the UT/LS O_3 composition from LNO_x and BB emissions and from dynamical processes is analyzed.

The DC3 field experiment and the data products are briefly described in section 2. A general overview of the CO and O_3 composition in selected wildfire plumes and their O_3-CO correlation are given in section 3. Three detailed thunderstorm case studies are presented in section 4 based on Falcon time series of a variety of trace species and the O_3-CO correlation within and in the vicinity of the thunderstorm outflow. The 30 May 2012 case focuses on the fresh supercell and MCC outflow over Texas and Oklahoma, whereas the 8 and 12 June 2012 cases focus on the aged MCS and fresh squall line outflow over Colorado and Kansas, respectively. In section 5 the pronounced O_3 gradients observed in the DC3 thunderstorm outflow region are discussed in detail. The summary and conclusions are given in section 6.

2. DC3 Field Experiment and Data Products

2.1. The DC3 Field Experiment Focusing on Falcon Measurements

A detailed overview of the DC3 field experiment is given by *Barth et al*. [2015]. For a detailed overview of previous studies on thunderstorms and chemistry over the U.S. and the motivation for the DC3 field experiment, see also *Barth et al*. [2015]. The DC3 field phase was carried out from 1 May to 30 June 2012 with three different aircraft platforms in operation and several ground-based observations. All three research aircraft, the NSF/NCAR Gulfstream-V (GV), NASA-DC8, and DLR-Falcon, were based at the airport in Salina, Kansas (38.8°N, 97.6°W). The Falcon performed mission flights in the time period 30 May to 17 June to Colorado, Wyoming, Nebraska, Missouri, Arkansas, Oklahoma, Texas, and New Mexico. For more details see HH2016. The aircraft was equipped with a variety of trace species instruments, see Table 1 herein. Our main target regions over the central U.S. were fresh and aged (0–12/12–24 h) anvil outflow in the UT up to 12.4 km altitude and fresh and aged plumes from wildfires in the lower, middle, and upper troposphere. The anvil outflow was probed from different types of convective systems, i.e., supercells, MCCs, MCSs, and squall lines (SQLs).

In the present study, we analyze a variety of in situ trace species measurements (CO, O_3, SO_2, CH_4, NO, NO_x, NO_y, CN, and rBC) sampled by the DLR-Falcon. During each flight several VOC samples were taken. In addition, a video camera was mounted in the Falcon cockpit monitoring the entire flight from start to landing. The videos were partly used to determine the in-cloud time sequences in the anvil outflow and the presence of smoke from wildfires. Further, the Falcon was equipped with a standard meteorological measurement system to measure position, altitude, temperature, pressure, humidity, and the three-dimensional wind vector (u, v, and w). These data were also needed for the calculation of the potential (Θ) and equivalent-potential temperature (Θ_e). For the computation of Θ_e for a water-saturation pseudo-adiabatic process, the formula suggested by *Bolton* [1980] was used for the Falcon data [see also *Huntrieser et al*., 2007]. All flight altitude values refer to pressure height and UTC (universal time coordinated) time. The time difference between UTC and the central daylight time (CDT) in Salina is +5 h (e.g., 06:00 CDT = 11:00 UTC).

2.2. Selection of DC3 Flight Planning Tools and Postanalysis Products

For the flight planning support and postanalysis of the airborne in situ data, a variety of meteorological products were available from the DC3 field catalog (http://catalog.eol.ucar.edu/dc3/).

Different kinds of visible and infrared/IR satellite products from the Geostationary Operational Environmental Satellite, GOES-13, were used in the present study, i.e., cloud top heights derived from the thermal-IR cloud top temperatures. Furthermore, GOES East—Aerosol/Smoke Products (GASP) were used for the monitoring of extensive smoke plumes (http://www.ssd.noaa.gov/PS/FIRE/GASP/), see also HH2016.

The location of the upper tropospheric tracer outflow from thunderstorms (e.g., LNO_x) was predicted on an hourly basis with the high-resolution Weather Research and Forecasting (WRF) ($\Delta x = 3$ km × 3 km) model from NCAR (http://ruc.noaa.gov/wrf/WG11_RT/) [see *Barth et al*., 2012]. The Lagrangian particle dispersion model FLEXPART was run to forecast the location of different natural (CO biomass burning) and anthropogenic

pollution sources (CO North America) in the lower/upper troposphere and as a column ($\Delta x = 0.5° \times 0.5°$) (http://transport.nilu.no/flexpart/) [see *Stohl et al*., 2003].

A tropospheric NO_2 product (80 km × 40 km) was available once a day at approximately noon CDT in near real time from the morning overpass of the Global Ozone Monitoring Experiment (GOME-2) instrument on the Meteorological Operational satellite programme (MetOp) satellite. These images were provided by NOAA National Environmental Satellite Data and Information Service (NESDIS) for the monitoring of LNO_x plumes (same retrieval algorithm as used in *Bucsela et al*. [2006]).

For the monitoring of the flight track during the field missions, the NCAR-Earth Observing Laboratory (EOL) operation tool was successfully used. The GOES-13 satellite images were overlaid by constant altitude plan position indicator images from the Next Generation Weather Radar (NEXRAD): a network of 160 high-resolution S band Doppler weather radars operated by the National Weather Service (http://www.roc.noaa.gov/WSR88D/). Furthermore, the NCAR-EOL operation tool offered the possibility to overlay lightning data from the National Lightning Detection Network (NLDN) and flight track data on the satellite images. The NLDN system is operated by the Vaisala Thunderstorm Unit [*Cummins and Murphy*, 2009]; http://thunderstorm.vaisala.com/. Similar images as the NCAR-EOL operation tool images are shown in the present study; however, in addition, O_3 distributions along the flight track have been superimposed.

Detailed radar measurements were performed from the ground in Oklahoma/Texas with the Shared Mobile Atmospheric Research and Teaching (SMART) single and dual polarized C band Doppler radars (SR1 and SR2) [*Biggerstaff et al*., 2005]. Multi-Doppler three-dimensional variational (3DVAR) data assimilation analyses of SMART and other available radar data were used to derive the vertical velocity within the storms. Here X-band dual polarized Doppler radar data from the mobile radar known as NOAA X-POL (NOXP) operated by T. Mansell, NOAA National Severe Storms Laboratory (NSSL), and data from the Dyess Air Force Base in Abilene were used. The analysis technique follows *Potvin et al*. [2012].

3. Falcon Observations in Wildfire Plumes

3.1. Influence From Wildfires

Some of the largest and most destructive wildfires in New Mexico (NM) and Colorado state's history were burning during the DC3 field experiment: the Whitewater-Baldy (NM), the Little Bear (NM), and the High Park Fire in Colorado, see Table 3 in HH2016 and details herein. Pollution layers from these wildfires, elevated in CO, SO_2, and rBC, were observed during most of the Falcon flights, not only at low altitudes but also in the UT up to ~10 km altitude (see Figure 2 herein). Occasionally, these BB emissions were transported upward in and/or nearby thunderstorms and observed within or just below the anvil outflow region as illustrated in Figures 16 and 17 herein. In Table 4 in HH2016, the most intense BB plumes probed by the Falcon (according to given criteria) and their mean and maximum trace species mixing ratios (CO, SO_2, and rBC) are listed. Furthermore, in this table information on date and time, fire source, distance from fire source, plume height (depth), and plume age is given.

In the present study we use these selected BB plumes from Table 4 in HH2016 and divide them into thinner layers where a clear O_3-CO correlation was observed. Their maximum O_3 and CO mixing ratios were determined; see Table 1 and references herein to single O_3-CO correlation plots presented later in section 4. The selected time sequences for the BB plumes are given in the legend of these correlation plots. In addition, in Table 1 a number of LNO_x plumes probed on these flights and a further case with anthropogenic pollution (8 June) were included which are discussed later in section 4.

3.2. The O_3-CO Correlation in Lofted Wildfire Plumes

Possible reasons for the highly variable O_3 and CO mixing ratios in the selected BB plumes and their O_3-CO correlation are discussed next. One way to identify cases with photochemical O_3 production or intrusions of O_3-rich air from the stratosphere is to focus on the O_3-CO correlation (section 1). In Figure 1, O_3-CO correlations from five selected DC3 thunderstorm flights are shown and colored according to flight date. Negative O_3-CO correlations (stratospheric air masses) were observed during all of these flights: especially pronounced on 3 May and 8 and 12 June. In contrast, positive O_3-CO correlations were frequently found in BB plumes from wildfires. CO mixing ratios exceeding ~170 nmol mol^{-1} were, in general, caused by especially pronounced BB

Table 1. $\Delta O_3/\Delta CO$ Ratios in Selected Layers Impacted by Anthropogenic Pollution, Biomass Burning Emissions From Wildfires and Lightning-Produced NO_x (LNO_x) During DC3 (in Italic/Bold: Plumes Not/Strongly Mixed With Stratospheric Air Masses) (Based On Table 4 in HH2016)

DC3 Flight Number, Date, Flight a or b	Source	Figure Number (Including Data Range)	Pressure Altitude (km)	Maximum CO Mixing Ratio (nmol mol^{-1})	Maximum O_3 Mixing Ratio (nmol mol^{-1})	Mix With Stratospheric Air Masses?	$\Delta O_3/\Delta CO$ Ratio
F#4 300512b	Baldy/Whitewater fire (NM)	1	*1.2–1.6*	*200*	*80*	*No*	*+0.10*
	Baldy/Whitewater fire (NM)	9a	8.5–8.7	130	90	Yes	+0.38
	Baldy/Whitewater fire (NM)	9a	9.9–10.4	120	100	Yes	+0.39
	Baldy/Whitewater fire (NM)	9a	at 10.4	**120**	**150**	**Yes**	**−1.67**
	LNO_x and Baldy/Whitewater fire (NM)	9b	at 9.1	160	130	Yes	+0.49
	LNO_x and Baldy/Whitewater fire (NM)	9b	9.1–9.4	130	140	Yes	+1.42
F#8 080612a	Anthropogenic pollution (TX)	24a	6.6–7.2	120	110	Yes	+1.44
	Anthropogenic pollution (TX)	24a	*7.4–7.9*	*120*	*70*	*No*	*+0.14*
	LNO_x and Anthropogenic pollution (TX)	24b	**8.8–10.7**	**110**	**160**	**Yes**	**−3.75**
	LNO_x and Anthropogenic pollution (TX)	24b	**at 11.6**	**110**	**280**	**Yes**	**−3.44**
F#11 110612b	Little Bear fire (NM)	1	*5.8–6.9*	*720*	*80*	*No*	*+0.03*
F#12 120612a	High Park fire (CO)	16	7.1–9.6	180	120	Yes	+0.44
	High Park fire (CO)	16	7.9–9.7	190	120	Yes	+0.38
	LNO_x and High Park fire (CO)	16	**11.0–11.9**	**130**	**260**	**Yes**	**−3.87**

plumes. From Figure 1 it is obvious that rather variable O_3-CO correlations were observed in the selected BB plumes on 30 May and 11 and 12 June. Some examples and explanations will be given below.

The change of O_3 over the change of CO ($\Delta O_3/\Delta CO$ ratio) is determined by finding the linear regression slope of the O_3-CO correlation and is summarized for selected BB plumes in Table 1. On 30 May, in the dense BB plume probed in the BL (1.2–1.6 km) during the descent to Lubbock (white dots), the $\Delta O_3/\Delta CO$ ratio (+0.1) indicated a rather low O_3 production rate ~600 km downstream from the New Mexico Whitewater-Baldy Fire. The plume age was determined to be <24 h with online HYbrid Single-Particle Lagrangian Integrated Trajectory (HYSPLIT) backward trajectories [*Draxler and Rolph*, 2014; *Rolph*, 2014] (http://ready.arl.noaa.gov/HYSPLIT.php), see also Table 4 in HH2016. Ozone mixing ratios were rather low in the plume and mainly varied between ~50 and 70 nmol mol^{-1}. On 11 June, similar conditions were observed in a BB plume lofted to 6–7 km (yellow dots); the $\Delta O_3/\Delta CO$ ratio (+0.03) was close to zero ~1000 km downstream from the New Mexico Little Bear Fire, and the plume age was determined to be ~24–27 h. Ozone mixing ratios were still rather low in the plume and varied between ~50 and 80 nmol mol^{-1}. In contrast, on 12 June (green dots), the $\Delta O_3/\Delta CO$ ratio (+0.4) was distinctly higher in a lofted BB plume (age ~9 h) probed in the UT (7–10 km) ~600 km downwind from the Colorado High Park Fire and O_3 mixing ratios reached up to ~120 nmol mol^{-1}.

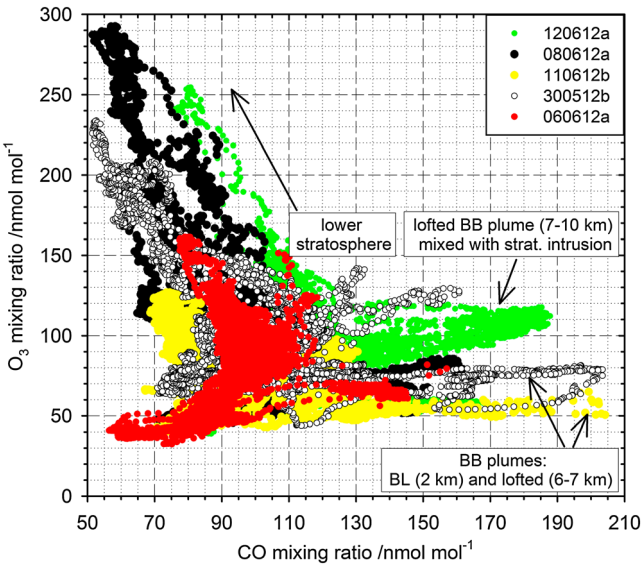

Figure 1. O_3-CO correlations for five selected DC3 flights where BB plumes (indicated) and thunderstorm outflow were probed (color coded according to date: ddmmyy). For a better overview, the *x* axis was cut at 210 nmol mol^{-1}, however on the flight 110612b measured CO mixing ratios in the BB plume exceeded ~700 nmol mol^{-1}.

The determined $\Delta O_3/\Delta CO$ ratios in polluted plumes (mainly from BB, LNO_x excluded) vary between +1.4 and −1.7 as listed in Table 1, with a tendency to distinctly higher positive values above ~8 km and one negative value at ~10 km. In the majority of the BB plumes probed by the Falcon below ~8 km, there is a tendency to a slightly positive correlation on the order of $\Delta O_3/\Delta CO =$ +0.1. In these plumes O_3 mixing ratios reach up to ~80 nmol mol^{-1} compared

to ~70 nmol mol^{-1} in the background (O_3 enhancement one day after emission: ~10 nmol mol^{-1}). According to the values presented in section 1, we suggest that photochemical production is the most likely source for O_3 enhancements observed in our BB plumes below ~8 km.

Higher up, at ~8–10 km, a distinct stepwise change and increase of the $\Delta O_3/\Delta CO$ ratio is observed toward values in the range of +0.4 (but also one negative value), indicative of a sudden change in processes influencing this ratio. In these UT-BB plumes, O_3 mixing ratios are generally in the range of 90–130 nmol mol^{-1} (compared to the background ~70–90 nmol mol^{-1}), suggesting both in-mixing from the stratosphere and/or photochemical O_3 production as possible processes. The observed O_3 enhancements in the UT-BB plumes are, however, partly higher than expected from photochemical O_3 production alone ($<$10 nmol mol^{-1} d, see section 1). For this reason, the major part of the observed O_3 enhancements in lofted BB plumes above ~8 km in the vicinity of thunderstorms would more likely be consistent with the wrapping of stratospheric intrusions around the thunderstorm outflow as recently observed by *Pan et al.* [2014] for another DC3 thunderstorm. In the next section three Falcon thunderstorm case studies will be analyzed in detail to support the hypothesis stated here.

4. Three Falcon Thunderstorm Case Studies

In the following, observations during the Falcon flight on 30 May and 8 and 12 June 2012 are described and discussed in detail.

4.1. The 30 May 2012: Fresh Supercell and MCC Outflow Over Texas/Oklahoma

4.1.1. Observations on 30 May 2012

On 30 May 2012 the Falcon performed two flights. The first flight was mainly dedicated to the smoke plume from the Whitewater-Baldy Fire in New Mexico (see Table 4 in HH2016). Emissions from the fire were probed downwind of the source region (~400–700 km) between Albuquerque (NM) and Amarillo-Lubbock (TX). The observed BB plume was most pronounced at ~2–5 km altitude (see Figures 2a, 2b, and 2e herein). At ~4 km, CO mixing ratios reached up to 540 nmol mol^{-1} (1 s values not shown). Increasing rBC mass mixing ratios with altitude were also measured from the ground to the middle troposphere (see Figure 2e herein), with a maximum value at ~4 km of 1508 ng kg^{-1} (10 s value not shown). This value is similar to rBC mass mixing ratios observed the day before in the same region (1477 ng kg^{-1}, BB plume at ~1–4 km) (Table 4 herein).

After a brief stop in Ardmore (OK), the second flight was dedicated to thunderstorm probing. Images from GOES East—Aerosol/Smoke Products (GASP) distinctly indicated that the New Mexican smoke plume was advected eastward in the evening of 30 May, crossed the Texas Panhandle and moved into western Oklahoma (Figure 2a). Similar to the setup the day before (29 May case in HH2016), two intense thunderstorm clusters developed in this area with the dense smoke plume (Aerosol Optical Depth (AOD) ~ 1.3): a huge MCC with several supercells east of the Texas Panhandle, along the Texas/Oklahoma border, and an isolated supercell near Abilene a few hundred kilometers west of Dallas. Both the probed MCC and the supercell were severe, triggered several tornadoes, and had very large hail as reported by the Storm Prediction Center in Norman, Oklahoma.

The thunderstorm systems mentioned above were characterized by high cloud tops with temperatures colder than −60°C, as indicated in the thermal-IR image from GOES-13 (http://catalog.eol.ucar.edu/cgi-bin/dc3_2012/ops/index). According to the GOES data, the average cloud top height of the anvil outflow deck of the MCC and supercell was ~11–13 km, however pronounced overshooting tops reached up to ~17–18 km (Figure 2b). The Mobile GPS Advanced Upper-Air Sounding System operated by the National Severe Storms Laboratory (NSSL) released a radiosonde in the prestorm environment (34.07°N, 99.39°W, border TX/OK) around 22 UTC which indicated a primary, secondary, and third tropopause at ~10.5, ~12.5, and ~15.5 km, respectively (http://data.eol.ucar.edu/). Later radiosonde temperature profiles from Fort Worth (TX) near Dallas (http://catalog.eol.ucar.edu/cgi-bin/dc3_2012/ops/index), Lamont (northern Oklahoma), and Dodge City (southwestern Kansas) for 31 May at 00 UTC showed a distinct large-scale double-tropopause structure with a primary and secondary tropopause located at ~11.5–12.5 km and at ~17 km, respectively [see also *Homeyer et al.*, 2014, Figures 3b and 9]. A similar heterogeneously structured tropopause was already observed the day before (29 May case in HH2016), which may have facilitated the development of very deep convective cells with overshooting tops.

During the first part of the second flight on 30 May, the Falcon headed southwestward from Ardmore (Figure 3a), ascending below the MCC outflow (according to the onboard video). Thereafter, the aircraft

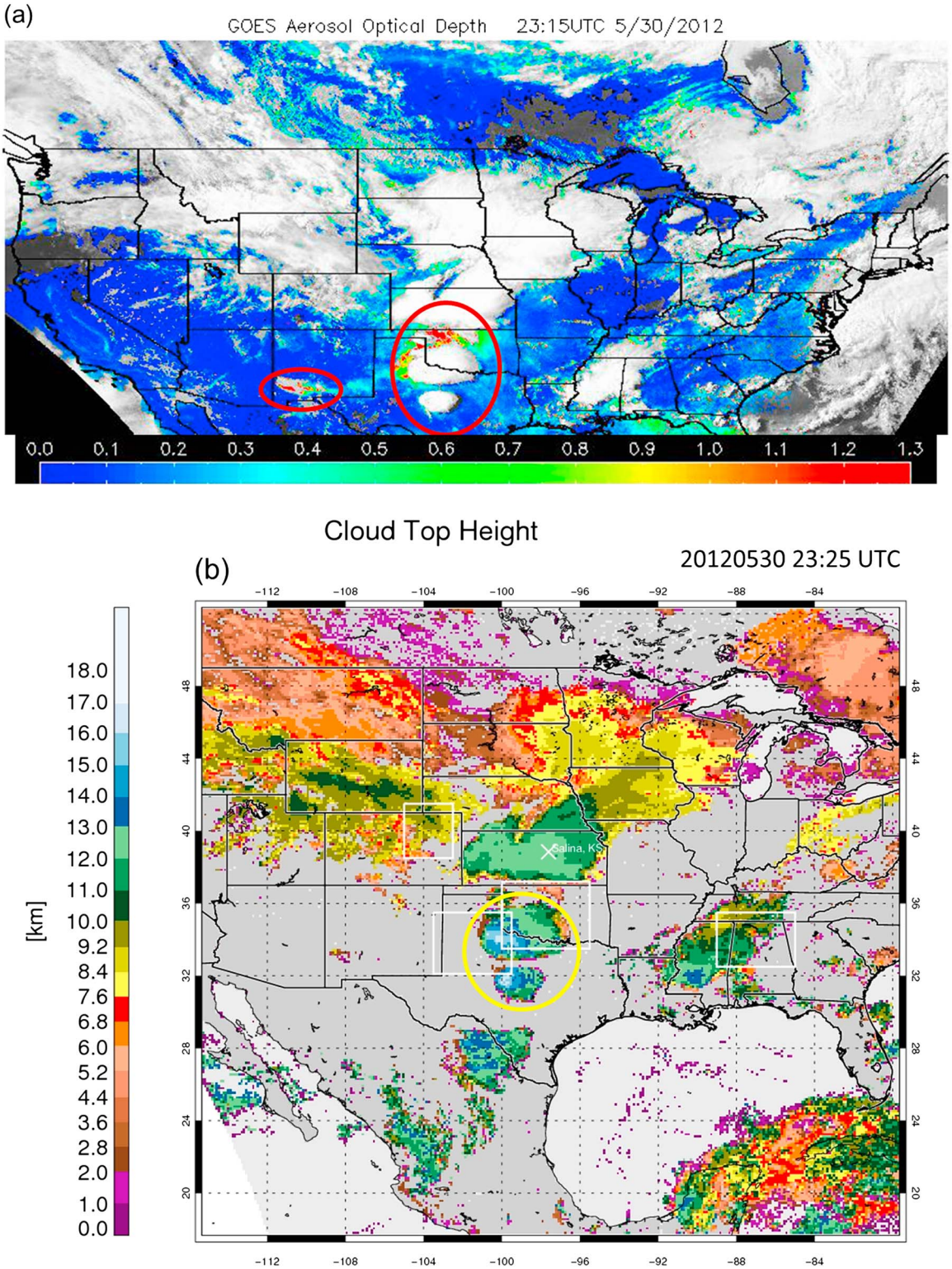

Figure 2. GOES Aerosol Optical Depth (AOD) over the U.S. and Canada on 30 May 2012 at 23:15 UTC (a). The left red circle indicates the source region of the Whitewater-Baldy fire (New Mexico), and the right red circle shows the area of aircraft operations (MCC and supercell over Texas/Oklahoma probed by the Falcon aircraft). Cloud top heights (in kilometer) derived from GOES data on 30 May 2012 at 23:25 UTC (b) (© NCAR/EOL). The yellow circle shows the area of the Falcon operations (supercell and MCC probed). The white squares mark the selected DC3 operation areas and the white cross the campaign base in Salina (KS).

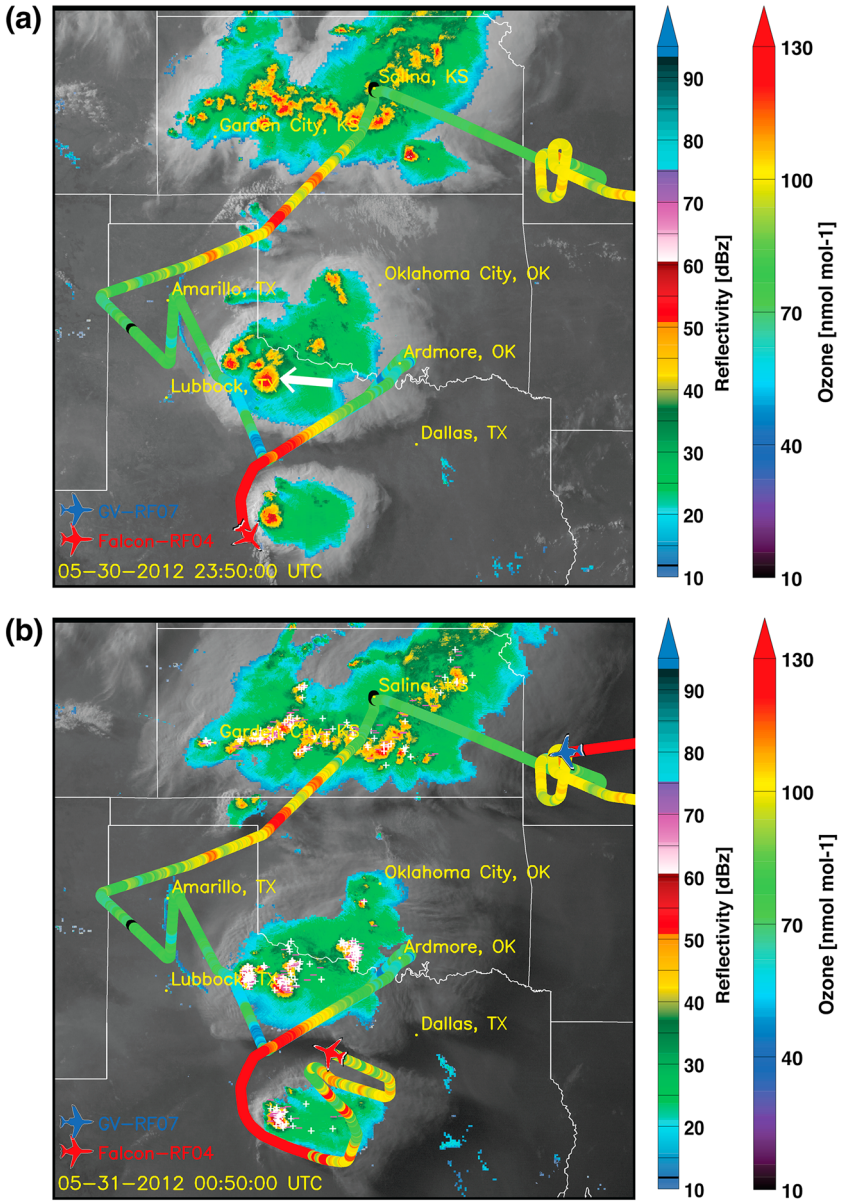

Figure 3. Flight tracks of the Falcon (red aircraft) in the evening on 30 May 2012 at 23:50 UTC (a) and 31 May at 00:50 UTC (b) to probe a smoke plume near Lubbock (TX), and after a brief stop in Ardmore (OK) to probe a MCC and an isolated supercell storm over Texas/Oklahoma (blue aircraft: GV). The flight tracks (color coded according to O_3 mixing ratios along the flight) are superimposed on a GOES IR satellite image (grey), NEXRAD reflectivity (colored clouds), and NLDN lightning data (white/pink plus/minus sign for positive/negative flashes). The white arrow marks a storm cell shown in more detail in Figures 5a and 5b. The smoke plume from the New Mexico Whitewater-Baldy Fire is visible near Lubbock.

circled counterclockwise around the supercell located just south of the MCC and crossed its dissipating outflow (Figure 3b). Thereby highly variable CO, O_3, and NO mixing ratios were observed as shown in the Falcon time series in Figures 4a and 4b, mainly impacted by emissions from wildfires, LNO_x, and stratospheric intrusions as discussed below in more detail.

During the ascent (Figure 4a, <85,500 s), the lower and middle troposphere up to 6 km was polluted by the Whitewater-Baldy smoke plume (CO mixing ratios up to 150 nmol mol^{-1}). Above the smoke plume, at ~6–8 km, typical background mixing ratios for both CO and O_3 were observed in the range of 70–80 nmol mol^{-1}. Between 8.5 and 10.4 km, as the aircraft was ascending just below the MCC anvil outflow and partly into the lower boundary of the outflow (Figure 3a), CO mixing ratios were elevated up to ~130 nmol mol^{-1} indicating

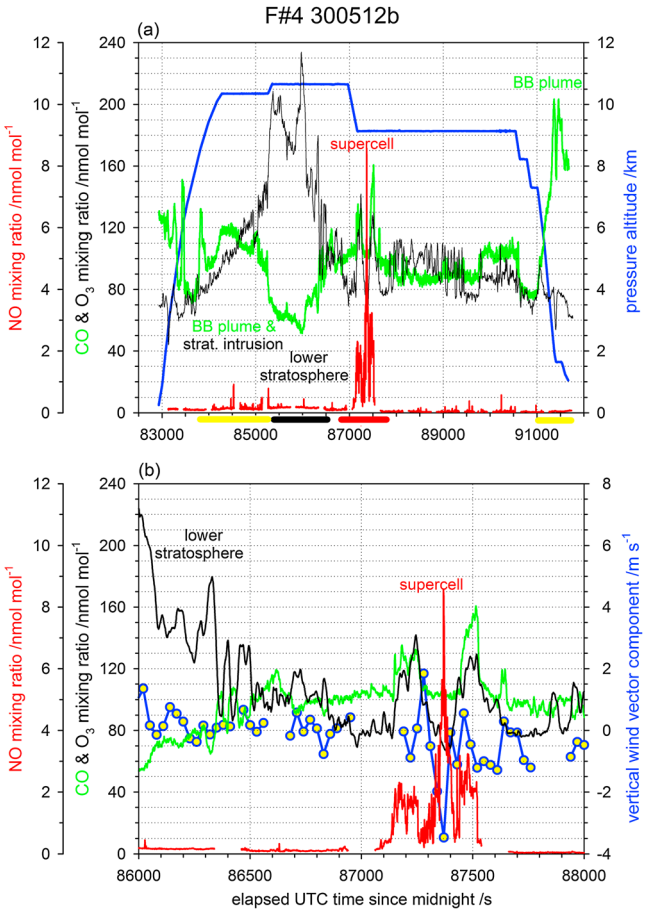

Figure 4. Time series of NO, CO, O_3, pressure altitude (all 1 s values), and vertical wind vector component (30 s mean) for the Falcon flight on 30 May 2012: (a) complete flight (b) and selected time period from 86,000 to 88,000 s. Positive vertical wind component values indicate downward motion. Colored bars in Figure 4a indicate selected time sequences of the flights with different air masses: BB plume (yellow), lower stratosphere (black), and fresh supercell outflow (red); see also Figures 9a and 9b.

traces of a lofted BB plume (83,819–85,250 s, 23:17–23:41 UTC). NO mixing ratios were still low here suggesting that the main MCC outflow (rich in LNO_x) was not probed during the ascent. Interestingly, O_3 mixing ratios continuously increased with altitude to stratospheric values (up to ~150 nmol mol^{-1} at 10.4 km, however still UT according to sounding data), as the aircraft ascended below the MCC outflow along the southern side of the storm. This indicates that the lofted BB plume most likely mixed with O_3-rich stratospheric air masses surrounding the MCC outflow as discussed later in section 4.1.2.

Evidence for the presence of a pronounced upper level downward motion within the MCC is available from multi-Doppler 3DVAR radar analyses. In Figures 5a and 5b data from the SMART radars and the Weather Surveillance Radar (WSR-88D) in Frederick (Oklahoma) on 30 May at 2330 UTC are combined. Two vertical cross sections (east-west and north-south) of the strongest supercell (white arrow in Figure 3a) embedded within the MCC are shown. Echo tops reached up to ~18 km. Along the edges of the main storm core dominated by strong updrafts (40–50 m s^{-1}), downdrafts (15–20 m s^{-1}) were particularly well developed on the western and southern side of the core, where the Falcon sampled. The main subsidence extended from 14 km to 10 km with a secondary region of subsidence down to ~8 km altitude. The centers of the maximum updrafts and downdrafts in the UT/LS region were located in a narrow region less than ~10 km apart, likely promoting a strong mixing of lower stratospheric air masses with tropospheric air masses from the BL not only inside the storm but also just outside the anvil outflow as observed by the Falcon.

At the rear side of the MCC, the Falcon passed the dry line. At a cruising altitude of 10.7 km (Figure 3a), O_3 mixing ratios were distinctly enhanced (~200 nmol mol^{-1}) and CO mixing ratios were low (50–80 nmol mol^{-1}) suggesting that the tropopause was located lower in this region (10.4 km) compared to the front side (10.7 km) and that the aircraft penetrated into the lowermost stratosphere (~85,000–86,500 s, Figure 4a). The two different tropopause altitudes are clearly visible in the vertical temperature profiles (T, Θ, and Θ_e) as illustrated in Figures 6a and 6b.

After the probing of the MCC, the Falcon headed further southwestward and probed an isolated supercell (Figure 3a). The aircraft circled around the isolated supercell and reached its front side (again UT), descending from 10.7 to 9.1 km to probe the dissipating anvil outflow (Figure 3b). In the vicinity and within the anvil outflow, a rapid change between updrafts and downdrafts dominated as illustrated by the vertical wind vector component (30 s mean) in Figure 4b. These time sequences are listed separately in Table 2, according to updrafts and downdraft dominated areas, to illustrate the major differences observed in a variety of measured trace species (CO, O_3, SO_2, and NO) due to dynamical effects.

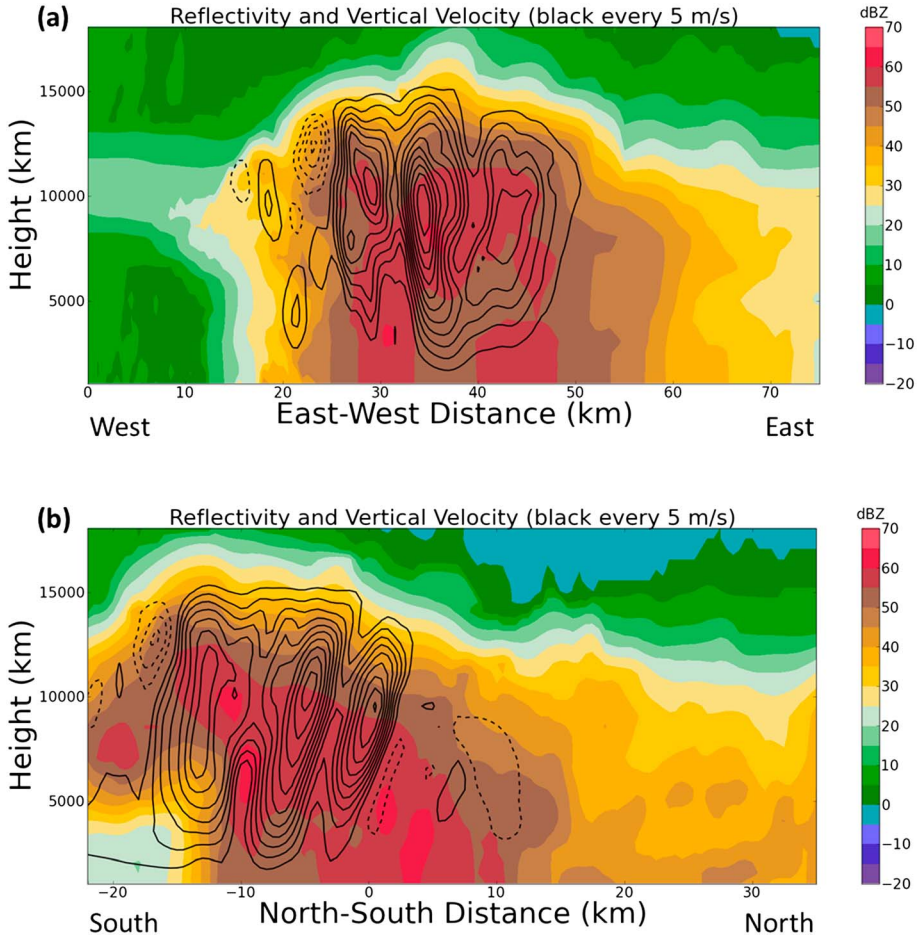

Figure 5. Radar reflectivity (dBZ) (colored) and vertical velocity (black isolines every 5 m s^{-1}, upward solid and downward dashed) obtained from multi-Doppler 3DVAR analysis of data from the SMART and NOXP radars on 30 May 2012 at 2330 UTC. (a and b) Vertical cross sections in east-west and north-south direction of the strongest supercell embedded in the MCC probed by the Falcon in Figure 3a marked by a white arrow. The grid center is the location of the SR1 radar (33.9°N, 100.3°W).

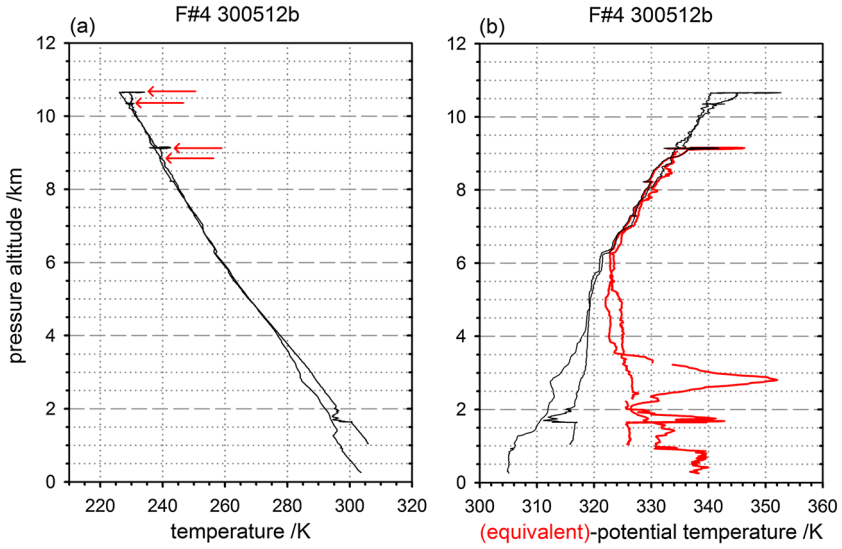

Figure 6. Vertical profiles of (a) temperature and (b) (equivalent)-potential temperature derived from Falcon measurements on 30 May 2012. The red arrows indicate two different tropopause levels at 10.4 and 10.7 km and stratospheric intrusions at 8.8 and 9.2 km.

Journal of Geophysical Research: Atmospheres

10.1002/2015JD024279

Table 2. Trace gas and Particle (Here Only SP2) Measurements in the Anvil Outflow on 30 May 2012 (Separated According To Anvil Regions With Updrafts or Downdrafts and the Mean Over the Entire Anvil Outflow in Italic)[a]

DC3 Flight Number, Date, Flight a or b, Anvil Time	Pressure Altitude (km)	CO Mixing Ratio (nmol mol^{-1})	O_3 Mixing Ratio (nmol mol^{-1})	SO_2 Mixing Ratio (pmol mol^{-1})	CH_4 Mixing Ratio (nmol mol^{-1})	NO Mixing Ratio (nmol mol^{-1})	NO_x Mixing Ratio (nmol mol^{-1})	NO_y Mixing Ratio (nmol mol^{-1})	Ethane/Propane (pmol mol^{-1}/ pmol mol^{-1})	Benzene/Toluene (pmol mol^{-1}/ pmol mol^{-1})	rBC[b] Mass Mixing Ratio (ng kg$^{-1)}$)
F#4 300512b (86,852–87,133 s) *upward*	10.3	103 ± 3 (97/110)	82 ± 5 (69/92)	45 ± 22 (8/101)	-	0.2 ± 0.1 (0.1/0.5)	-	-	-	-	-
F#4 300512b (87,134–87,323 s) *downward*	9.2	117 ± 10 (99/135)	108 ± 17 (75/142)	33 ± 16 (8/69)	-	1.2 ± 0.6 (0.2/2.3)	-	-	-	-	-
F#4 300512b (87,324–87,440 s) *upward*	9.1	103 ± 2 (100/107)	80 ± 13 (67/114)	55 ± 17 (19/82)	-	2.7 ± 1.8 (0.4/8.6)	-	-	-	-	-
F#4 300512b (87,441–87,577 s) *downward*	9.1	130 ± 19 (103/161)	113 ± 11 (92/129)	72 ± 29 (14/131)	-	2.3 ± 0.4 (1.1/3.2)	-	-	-	-	-
F#4 300512b (87,578–87,838 s) *upward*	9.1	98 ± 6 (89/120)	82 ± 7 (76/100)	52 ± 25 (6/117)	-	0.05 ± 0.01 (0.03/0.08)	-	-	-	-	-
F#4 300512b (86,852–87,838 s)	***9.5 (9.1–10.7)***	***↑108 ± 14***	***↑91 ± 17***	***50 ± 25***	**-**	***↑1.0 ± 1.3***	**-**	**-**	**-**	**-**	**–**
Background (83,988–84,040 s)	**9.4–9.6**	**97 ± 2**	**86 ± 4**	**50 ± 24**	**-**	**0.05 ± 0.03**	**-**	**-**	**247/29 = 8.5**	**5/27 = 0.2**	**-**

[a]Mean mixing ratios and standard deviations are given. Minimum and maximum mixing ratios are given in brackets. In addition, mean background mixing ratios outside the anvil outflow are given in bold. The arrows indicate if the anvil mixing ratios are higher (↑) or lower (↓) than the background mixing ratios.
[b]rBC = refractory black carbon.

At ~87,000 s (Figure 4b), the aircraft was first flying just below the supercell outflow, outside of clouds (according to the onboard video). NO mixing ratios were not enhanced; however, CO mixing ratios were slightly enhanced (~110 nmol mol^{-1}), and O_3 mixing ratios were rather low (70–80 nmol mol^{-1}) indicating that remnants of pollution were probed (according to FLEXPART most likely lofted BB plume and not anthropogenic pollution, see DC3 field catalog). Unfortunately, rBC measurements are not available for this time sequence. As the Falcon penetrated into the visible anvil outflow between 9.6 to 9.1 km altitude, strong gradients in CO, O_3, and NO mixing ratios were observed (Figure 4b). The edges of the dissipating anvil outflow partly had trace gas signatures of downward motion (~87,200–87,300 and ~87,400–87,500 s), as also confirmed by the vertical velocity. Ozone mixing ratios were elevated up to ~140 nmol mol^{-1}, as typical for the lowermost stratosphere, over a horizontal distance of ~20–40 km. In contrast, within the center of the anvil outflow (~87,300–87,400 s), O_3 mixing ratios were as low as ~70 nmol mol^{-1}, indicating upward motion from lower levels closer to the convective core, as also confirmed by the vertical velocity. Interestingly, the highest CO mixing ratios up to ~160 nmol mol^{-1} were observed along the edges of the anvil outflow dominated by downward motion (discussed in more detail in section 4.1.2). The highest NO mixing ratios (8.6 nmol mol^{-1}) were observed within the part of the anvil outflow dominated by upward motion (fresh NO production by lightning).

As listed in Table 2, SO_2 mixing ratios within the anvil outflow were ~50 pmol mol^{-1} on average (in bold italic) and similar to background conditions (in bold). The background ethane and propane mixing ratios at 9.5 km altitude were low with 247 and 29 pmol mol^{-1}, respectively, and the benzene/toluene ratio was 0.2, both indicating rather clean background conditions. Unfortunately, no VOC samples were taken within the anvil outflow during this flight. Due to the high humidity within the anvil outflow, no refractory black carbon (rBC) measurements were available during these flight sequences. Furthermore, CH_4, NO_x, and NO_y measurements were not available for this entire flight due to technical problems (see Table 2 in HH2016).

After passing the supercell, the aircraft continued heading northwestward at 9.1 km altitude and approached the anvil outflow of the MCC again (Figure 3b). In the clear air between the supercell and the MCC outflow (~89,500 s), O_3 and CO mixing ratios dropped below ~80 and ~90 nmol mol^{-1}, respectively, typical background values (Figure 4a). Thereafter, the lower boundary of the MCC outflow was sampled again (~90,000 s), O_3, and CO mixing ratios increased to values around 90–100 and 100–110 nmol mol^{-1}, respectively, influenced by the lofted BB plume and most likely mixing with stratospheric air masses as described before. The vertical temperature profiles indicate that stratospheric intrusions reached down to 8.8 and 9.2 km, visible as inversion layers (Figures 6a and 6b).

As the Falcon left the MCC outflow, it started to descend for landing in Lubbock. During the first part of the descent in clear air, between 9 and 7 km, both O_3 and CO mixing ratios dropped down to 70–80 nmol mol^{-1}, typical background values as observed during the ascent. Below 7 km, the advected BB plume from New Mexico was prominent again, especially pronounced between 3 km and the ground, with enhanced O_3 and CO mixing ratios, ~80–90 and up to ~200 nmol mol^{-1} (1 s values), respectively. Compared to the start in Ardmore, the BB plume was much more pronounced around Lubbock, due to the proximity to the source region.

4.1.2. Discussion of 30 May 2012 Observations

From the observations during the second Falcon flight on 30 May, it is obvious that especially strong upward and downward motions, within and in the vicinity of the supercell and MCC outflow, efficiently redistributed the chemical composition ratio in the UT/LS region. Schematics of the observations presented in the last subsection are summarized in Figure 7a for the supercell and in Figure 7b for the MCC and discussed in more detail below.

Almost the entire horizontal extent of the supercell outflow (Figure 3b) was probed from south to north but mainly the lower boundary near ~9 km, as indicated by the orange shading in Figure 7a. The entire cloud deck extended from ~9 to 11 km altitude. In the vicinity of the convective core of the supercell, updrafts dominated the vertical transport of CO-rich (BB plume, broad yellow arrow) and low-O_3 air masses from below (broad green arrow). Due to the strong intensity of the supercell (overshooting top), the uplifted BB emissions (from below 3 km according to the background O_3-CO composition in the LT) penetrated through the tropopause and mixed with LMS air masses (black yellow ellipse). O_3-rich but also CO-rich air masses were transported downward again along and into the edges of the overshooting top (curved yellow and straight

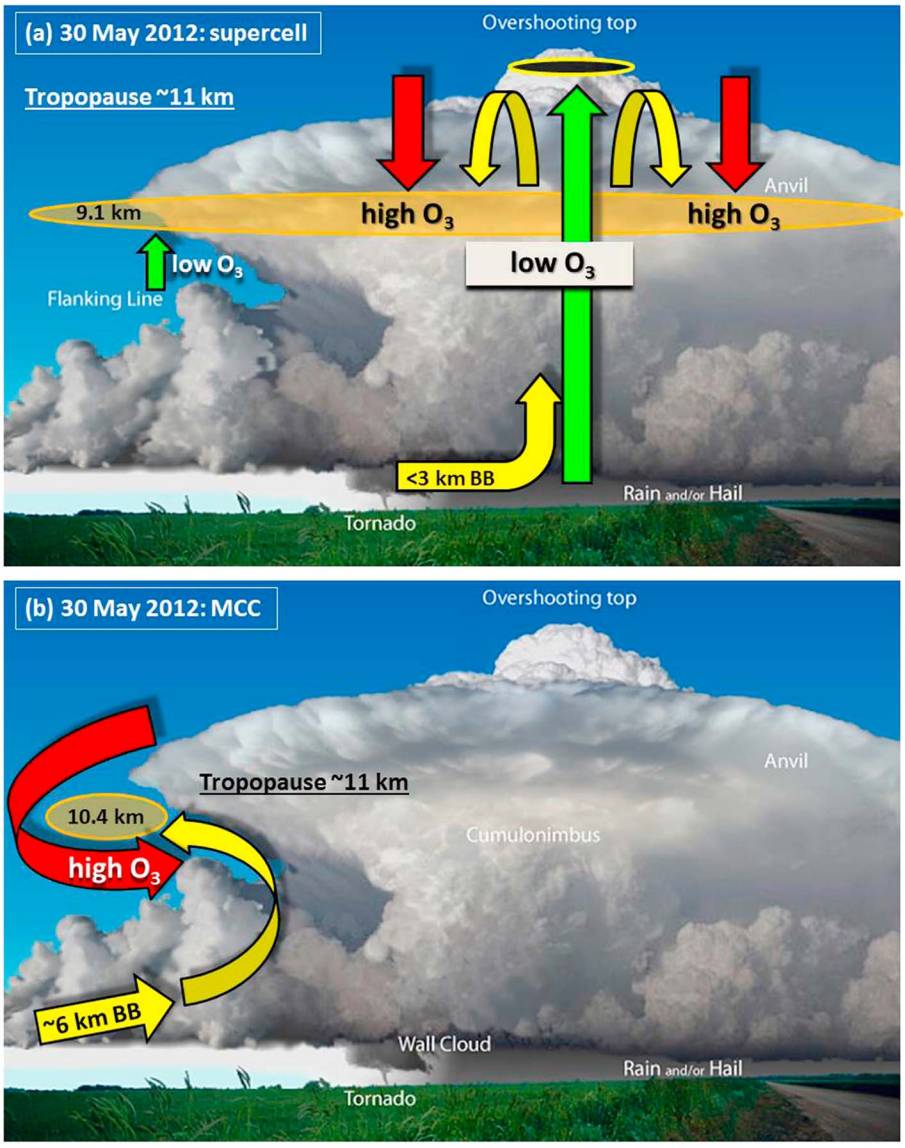

Figure 7. Schematic of an isolated, overshooting thunderstorm cell (credit: NOAA National Weather Service, http://www.srh.noaa.gov/jetstream/tstorms/tstrmtypes.htm). Superimposed are the major air mass transport pathways (colored arrows) observed during the Falcon flight on 30 May 2012 based on in situ trace gas measurements (CO and O_3) in the lower boundary of the outflow from a (a) supercell and below the outflow from a (b) MCC (orange shaded areas). In Figure 7 a emissions from wildfires (BB) and low O_3 mixing ratios are ingested into the supercell (yellow and green). Strong updrafts and downdrafts within the storm redistribute the ingested pollution (accumulation at the cloud top, black shaded area). As a response to the overshooting top, stratospheric air masses are transported downward into the anvil outflow (red). In Figure 7b emissions from wildfires (BB, yellow) are ingested into towering cumulus along the flanking line of the overshooting MCC and mix with a stratospheric intrusion wrapped around the anvil outflow (red).

red arrows), as compensation to the strong updrafts in the storm core. Normally, the CO mixing ratio rapidly decreases above the tropopause, which should cause a decrease in CO mixing ratios of the air masses transported downward. However, we observed the opposite in this specific case. We assume that a considerable amount of CO was already injected to the LMS earlier by the isolated supercell but also by the nearby overshooting MCC; the latter system was even more intense and higher than the isolated supercell (Figure 2b). The GOES aerosol optical depth image (Figure 2a) shows that the center of the strong Whitewater-Baldy smoke plume passed just below the MCC. Most likely, a high amount of CO was transported upward to the LMS by this MCC but also by the nearby isolated supercell and mixed with CO-poorer

but O_3-rich air masses. This mixture still enhanced both in CO and O_3 was later brought down again by the storm's downdrafts as seen in our measurements. Our hypothesis on these transport pathways is supported by the multi-Doppler radar analysis described before, where strong updrafts (~50 m s^{-1}) and downdrafts (~20 m s^{-1}) observed within a MCC supercell have the capability to very rapidly (~5–15 min) mix tropospheric and stratospheric air masses.

Besides these measurements inside the anvil outflow of the supercell, measurements just outside of the outflow are also illustrated in Figure 7a. Compared to the UT background, CO and O_3 mixing ratios were higher and lower within this cloud-free air, respectively, indicating that pollution transport from below was efficient, not only inside the storm but also just outside of the storm (low O_3 indicated by thin green arrows in Figure 7a). Around 87,750 s, within this cloud-free air close to the storm at ~9 km, O_3 mixing ratio as low as ~80 nmol mol^{-1} and slightly elevated CO mixing ratios (~100 nmol mol^{-1}) were observed, indicative of pollution transport from the BL. In addition, elevated water vapor mixing ratios (0.3–0.4 g kg^{-1}) and relative humidity values (~60%) indicate that these air masses were possibly uplifted from lower levels. Most likely, smaller convective cells (towering cumulus along the flanking line) uplift and spread BB emissions just below the anvil outflow (yellow arrows in Figure 7b), as discussed in HH2016 and illustrated in Figures 13, 16, and 17 herein. In the present study Figure 8 nicely shows that an extended area of pronounced wave clouds was present east of the investigated thunderstorms supporting the uplift of BB emissions. The exceptional high equivalent potential temperature observed at ~3 km altitude (>350 K) may also facilitate the rapid lifting of such BB layers to the UT (Figure 6b).

In the MCC case (Figure 7b) the main anvil outflow deck spread slightly higher compared to the supercell case (MCC main ceiling at ~12–13 km, clearly located above the primary tropopause). Stratospheric air masses were likely forced to move downward as compensation to the powerful upward motion in the MCC penetrating the tropopause. Our in situ measurements indicate that these stratospheric air masses likely enwrapped the anvil outflow (red curved arrow) similar to the findings by *Pan et al.* [2014] and mixed with CO-rich air masses located just below the MCC outflow (lofted BB plume, yellow arrows).

A further illustrative example of the mixing of the lofted BB plume with air masses of stratospheric origin wrapping around the MCC outflow is presented in Figure 9a showing the O_3-CO correlation. For comparison, the correlation in the free tropospheric and stratospheric background is superimposed in gray (from Falcon a-flight on 8 June 2012). As described before, during the westward ascent, just below the MCC outflow, both CO and O_3 mixing ratios increased with altitude between 8.5 and 10.4 km (Figure 4a). In Figure 9 a positive O_3-CO correlations ($\Delta O_3/\Delta CO$ ratio = +0.4) were observed within this lower portion of the BB plume (yellow dots with no or light orange edges), mainly due to mixing with the stratospheric intrusion and not due to photochemical O_3 production. The ratio value alone (also listed in Table 1) is within common ranges reported in BB plumes affected by photochemical O_3 production (section 1). However, the steep increase in O_3 mixing ratios with altitude (Figure 4a) clearly suggests that O_3-rich air masses from the LMS are mixed in which explain the enhanced $\Delta O_3/\Delta CO$ ratio observed. Photochemical O_3 production within the plume is not expected to increase with altitude, as the production rate is slower at colder temperatures.

Within the upper portion of the BB plume (~10.4 km), at the rear side of the MCC, a negative O_3-CO correlation ($\Delta O_3/\Delta CO$ ratio = −1.7) was observed (yellow dots with thick black edges in Figure 9a), dominated by the in-mixing of the BB plume into the LMS. South of the MCC, as the aircraft ascended up to 10.7 km and circled counterclockwise around the supercell, the aircraft penetrated into the troposphere again, indicating that the local tropopause was slightly higher in this region (tilted tropopause between thunderstorm front and rear side supporting the troposphere-stratosphere exchange) (Figures 6a and 6b). The anvil outflow of the supercell (characterized by elevated NO) was probed next which was located distinctly lower, at 9.1–9.4 km (Figure 4b). Mixing of the outflow with both stratospheric and BB impacted air masses was prominent (for illustration see Figure 7a), which caused a positive O_3-CO correlation, as shown in Figure 9b. During the descent from 9.4 to 9.1 km, the regression slope was steeper ($\Delta O_3/\Delta CO$ ratio = +1.4) (red dots without black edges) compared to the correlation at the cruise altitude of 9.1 km ($\Delta O_3/\Delta CO$ ratio = +0.5) (red dots with black edges), due to increasing influence of stratospheric air masses and decreasing influence of the ingested BB plume at the higher level. The high CO mixing ratios (~160 nmol mol^{-1}) observed within the anvil outflow indicate that BB emissions were most likely ingested into the supercell from the top of the BL at ~3 km

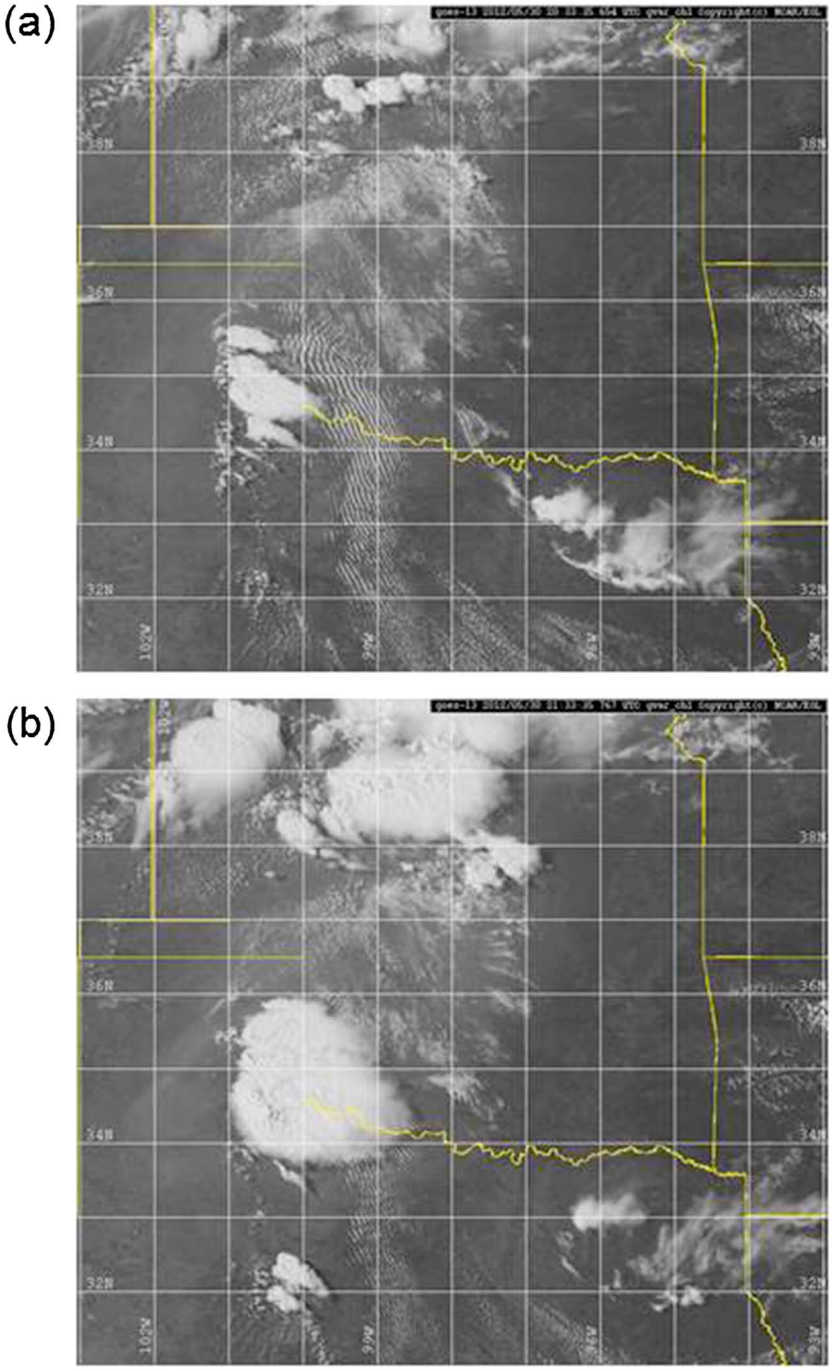

Figure 8. GOES visible satellite images on 30 May 2012 at (a) 20:33 UTC and 30 May 2012 at (b) 21:33 UTC (© NCAR/EOL). Along the flanking line of the probed thunderstorms extended wave cloud formations are visible in Figure 8a which are later in Figure 8b covered by the anvil outflow.

(according to CO and Θ_e values in Figures 4a and 6b, respectively). In addition, the observed elevated O_3 mixing ratios (~140 nmol mol^{-1}) suggest that air masses were simultaneously transported downward from the tropopause region (10.4–10.7 km or above) into the anvil (values too high values for photochemical O_3 production).

In Table 2, average trace gas conditions in the supercell outflow (bold italic) and typical background mixing ratios (bold) are listed. Both CO and O_3 mixing ratios were on average distinctly enhanced in the anvil outflow

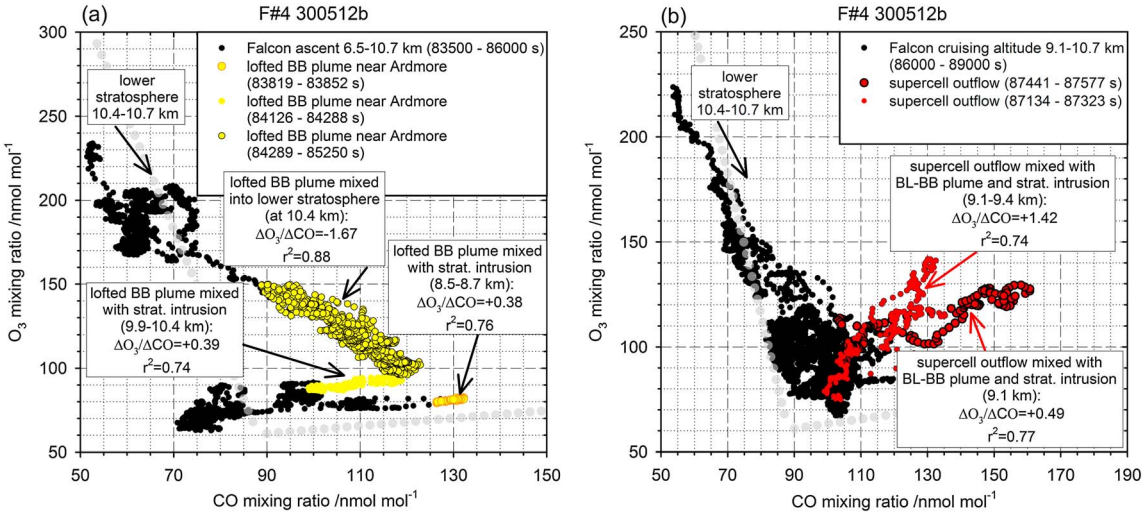

Figure 9. (a) O_3-CO correlations during the Falcon flight on 30 May 2012 for the time period of the ascent from Ardmore. (b) The correlations in the lofted BB plume are marked with yellow dots. O_3-CO correlations during the Falcon flight on 30 May 2012 for the time period of the cruising at 9.1–10.7 km. The correlations within the anvil outflow of the supercell are marked with red dots. The correlation in the free tropospheric and stratospheric background is marked with light gray dots.

by 11 and 5 nmol mol^{-1}, respectively, compared to the background composition. In summary, like the lofted BB plume in Figure 9a, the observed O_3 enhancement within the LNO_x plume (Figure 9b) was mainly caused by downward mixing of O_3-rich air masses from the LMS and not due to photochemical O_3 production. The highly variable $\Delta O_3/\Delta CO$ ratios with altitude observed in the probed LNO_x plume also suggest a major dynamical and not photochemical influence. The observed trace gas gradients in the time series have larger amplitudes than expected from chemical processes only. As discussed in section 1 such chemical processes are also much slower.

4.2. The 12 June 2012: Fresh Squall Line Outflow Over Colorado/Kansas

4.2.1. Observations on 12 June 2012

On 12 June 2012 a pronounced smoke plume from the High Park Fire in Colorado (see Tables 3 and 4 in HH2016) spread southeastward along the border between Colorado and Kansas according to the FLEXPART lower tropospheric BB tracer analyses (CO) (Figure 10). In addition, BB emissions from the wildfires in New Mexico likely spread northeastward to the same region.

An elongated squall line (~700 km anvil length) with cold cloud tops (< -60°C) developed in the convergence zone of these smoke plumes along the border between Kansas, Oklahoma, and Colorado (http://catalog.eol.ucar.edu/cgi-bin/dc3_2012/ops/index), the target area for the Falcon flight on 12 June. The average cloud top height was in the range of 12–13 km, with overshooting tops up to 14–15 km (Figure 11). The cloud tops were not as high as observed during the previously presented flight (30 May). The 00 UTC radiosoundings from Dodge City (southwestern KS) and Amarillo (Texas Panhandle) both indicate that the primary tropopause was located at 11.1 km (http://catalog.eol.ucar.edu/cgi-bin/dc3_2012/ops/index). In addition, in Dodge City a secondary tropopause was prominent at 11.8 km. Both tropopause heights are located slightly below the average cloud top height (~12–13 km), which indicates that the main cloud deck likely penetrated into the LMS.

After takeoff in Salina, the aircraft headed southwestward and remained in the lower troposphere (~3–5 km) to probe the smoke plume from the High Park (and NM) fire and the inflow region of the squall line (Figures 12a and 12b). Within this lower portion of the advected smoke layer (~79,500 s), the highest CO mixing ratios (~160 nmol mol^{-1}) were observed at 3.3 km altitude, whereas O_3 mixing ratios were rather low, in the range of 60 nmol mol^{-1}, indicating no pronounced photochemical O_3 production (Figure 13a). In addition, SO_2 and CH_4 mixing ratios were enhanced with ~0.5 nmol mol^{-1} and 1.90 μmol mol^{-1}, respectively (Figures 13c and 13d).

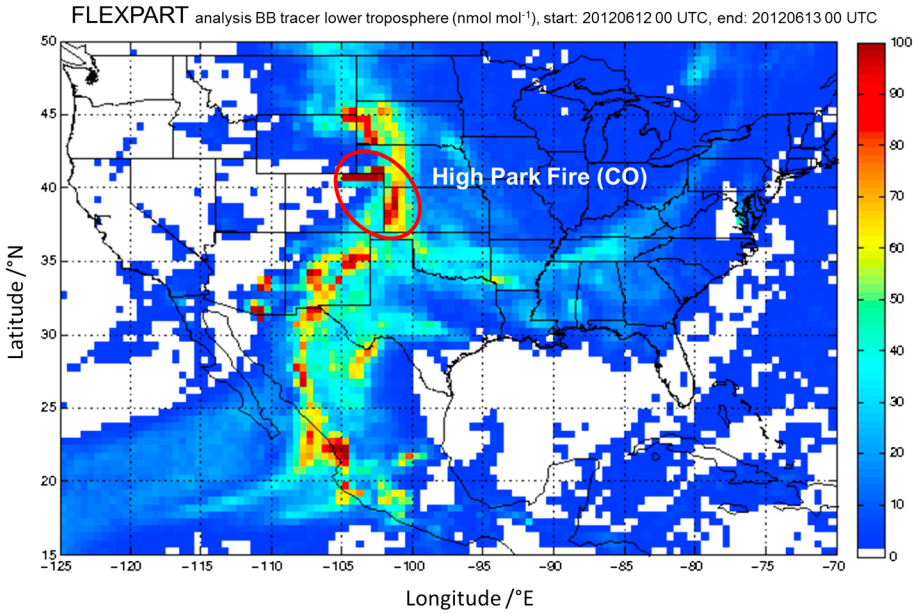

Figure 10. FLEXPART BB tracer analysis for the lower troposphere over the U.S. and Mexico. Begin and end of the simulation: 12 June at 00 UTC and 13 June at 00 UTC, 2012, respectively. Simulated BB-CO mixing ratios (in color) are given in nmol mol^{-1}. The red circle indicates the High Park fire in Colorado and the advection of the smoke plume toward the south along the border between Colorado and Kansas.

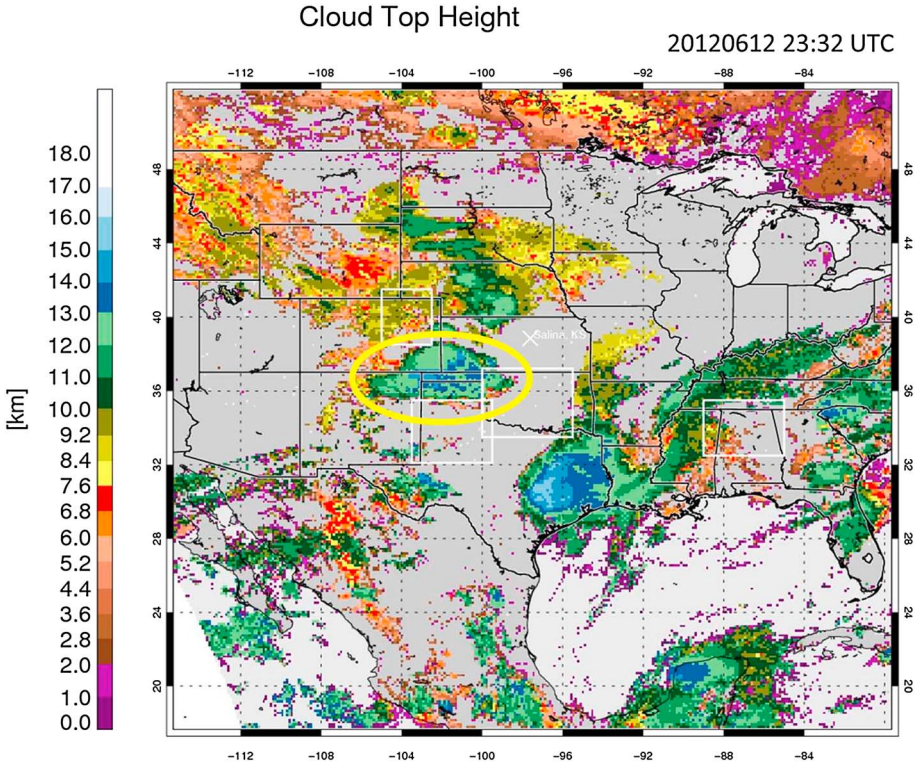

Figure 11. Cloud top heights (in kilometer) derived from GOES data on 12 June 2012 at 23:32 UTC (© NCAR/EOL). The yellow circle shows the area of the Falcon operations (squall line probed). The white squares mark the selected DC3 operation areas and the white cross the campaign base in Salina (KS).

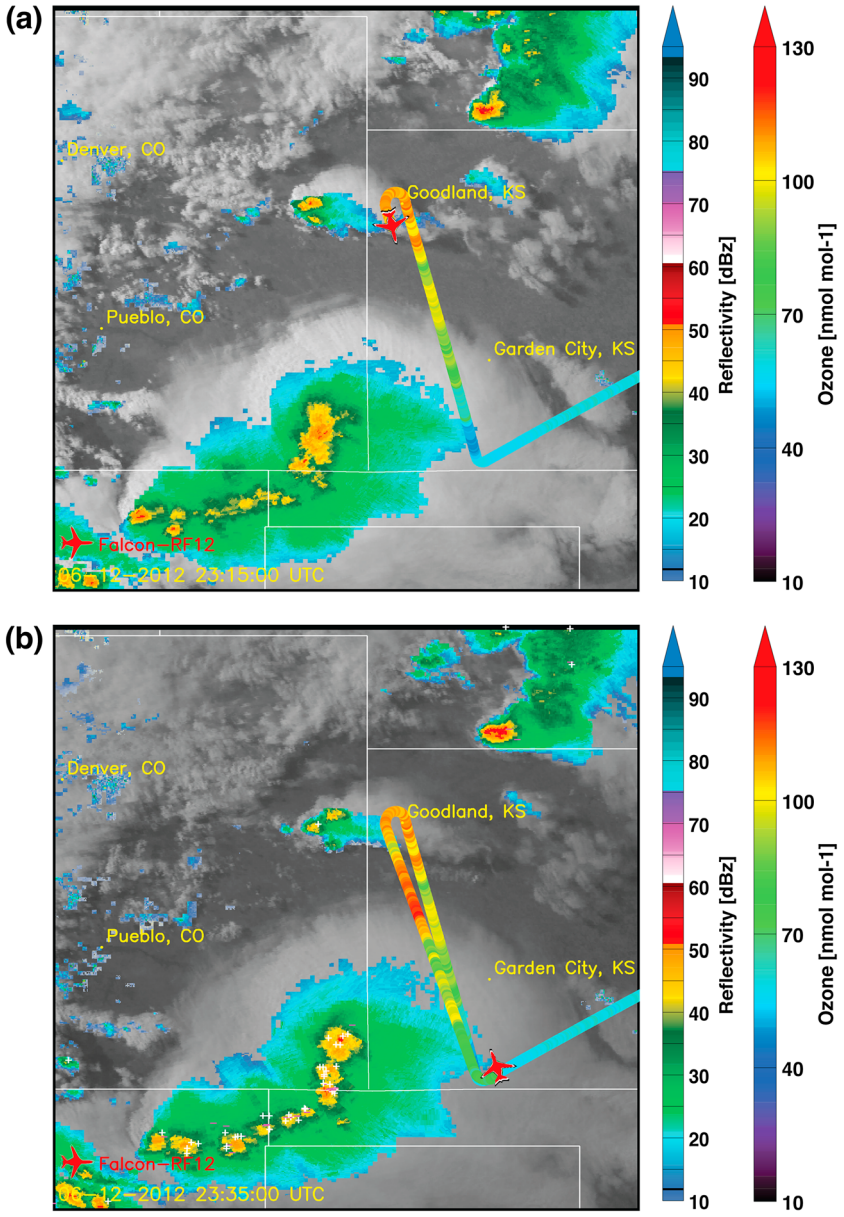

Figure 12. (a and b) Flight tracks of the Falcon (red aircraft) in the evening on 12 June 2012 at 23:15 UTC and at 23:35 UTC. After the start in Salina, the Falcon approached a squall line, located along the border between Kansas, Oklahoma and Colorado, at low altitudes. Below the anvil outflow the aircraft started to ascend in northerly direction and several cross sections in north southerly direction followed at different altitudes below, inside, and outside the anvil outflow. The flight tracks (color coded) are superimposed on a GOES IR satellite image (grey), NEXRAD reflectivity (colored clouds), and NLDN lightning data (white/pink plus/minus sign for positive/negative flashes). The flight tracks are color coded according to O_3 mixing ratios along the flight.

As the aircraft reached the squall line, it started to ascend below the anvil outflow, thereby also heading northward toward a smaller, isolated thunderstorm cell (Figure 12a). In the middle troposphere between 5 and 7 km, low CO and O_3 mixing ratios in the range of 80–90 nmol mol^{-1} and 50–60 nmol mol^{-1}, respectively, were observed as typical for the background (Figure 13a). During the previous flight (30 May) described in the last subsection, the same type of layer with low CO and O_3 mixing ratios was observed between 6 and 8 km. On 12 June, the layer above 7 km and below 9.7 km was characterized by strongly elevated CO and O_3 mixing ratios, up to 190 and 120 nmol mol^{-1}, respectively (~82,500–84,000 s). The vertical (equivalent)-potential temperature profiles indicate that an air mass layer located at ~3–4 km altitude, characterized by elevated Θ_e temperatures (~335 K), would have the potential to be uplifted to these altitudes in the UT (Figures 14a and 14b).

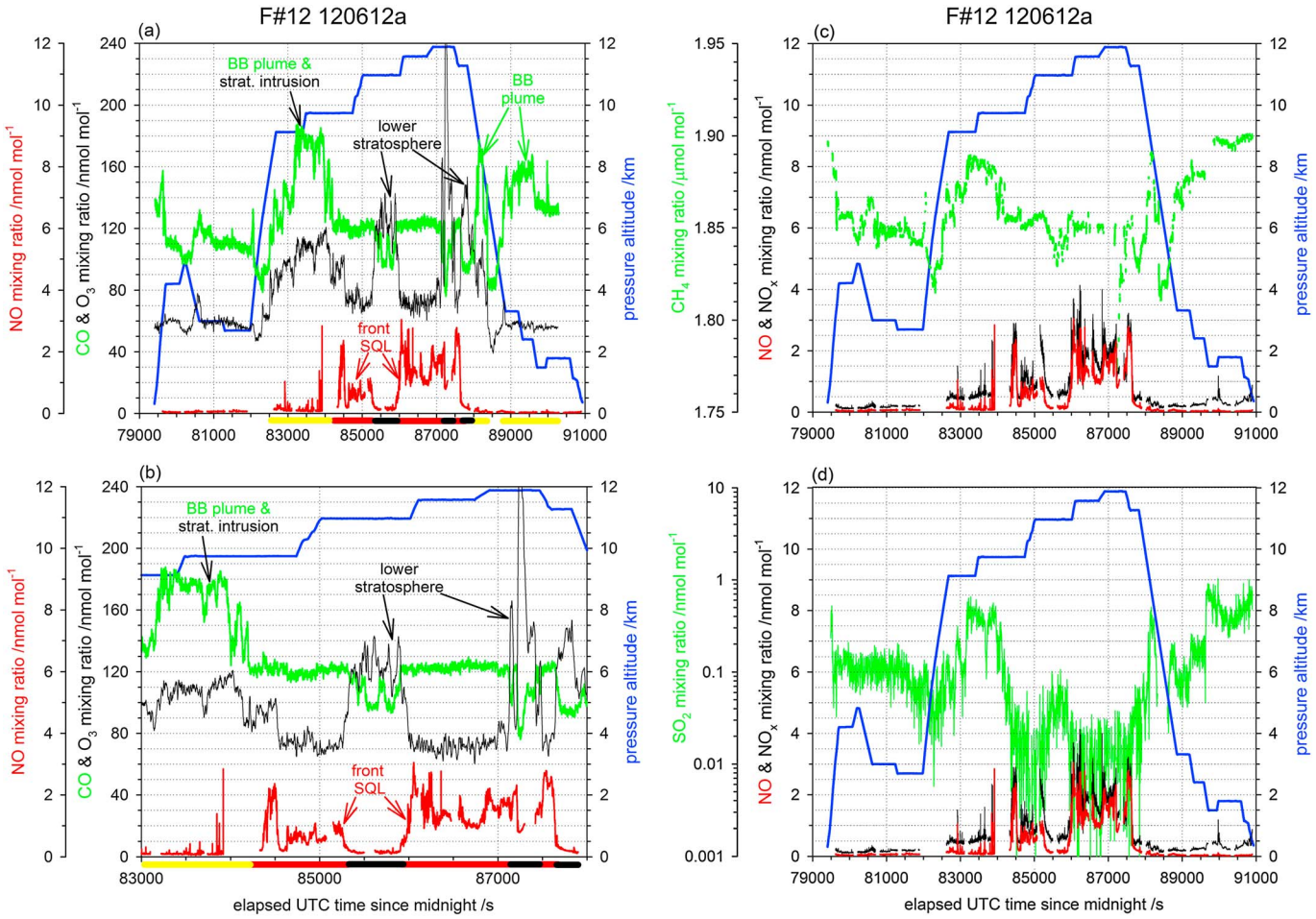

Figure 13. Time series of NO, NO_x, CO, O_3, SO_2, CH_4, and pressure altitude for the Falcon flight on 12 June 2012: (a, c, and d) complete flight and (b) selected time period from 83,000–88,000 s. Colored bars in Figures 13a and 13b indicate selected time sequences of the flight with different air masses: BB plume (yellow), stratospheric intrusion/lower stratosphere (black), and fresh squall line (SQL) outflow (red), see also Figure 16.

The aircraft then (after 84,000 s) started to probe the northeastern edge of the squall line outflow during stepwise ascent from 9.7 to 11.9 km altitude. Thereby, the aircraft was cruising between the squall line, background air and the smaller, isolated thunderstorm cell in the north (Figures 12a and 12b). Within the anvil outflow (Figure 13b: ~84,500–85,000 and ~86,000–87,000 s), elevated CO and low O_3 mixing ratios were observed, in the range of 120 and 70 nmol mol^{-1}, respectively, indicating upward transport from lower altitudes below ~4 km. In addition, NO and NO_x mixing ratios were distinctly enhanced within the anvil outflow (Figures 13a–13c), mainly due to in situ production by lightning. Along the northern edge of the anvil outflow, the lofted BB plume was most prominent in a layer between ~7 and 9.7 km. Above ~8 km and up to 9.7 km (~82,500–84,000 s) O_3 mixing ratios were, in addition, enhanced. As in the previous thunderstorm case described, no significantly elevated NO and NO_x mixing ratios were observed within this lofted BB. Most likely, the BB emissions were not uplifted inside the storm cell but near the active thunderstorm by flanking convection (see visible satellite images 1 km resolution, http://catalog.eol.ucar.edu/cgi-bin/dc3_2012/ops/index), as also illustrated for the previous case in Figure 8a. The high SO_2 and CH_4 mixing ratios observed within the UT-BB plume (~0.6 nmol mol^{-1} and 1.89 µmol mol^{-1}), similar to the composition observed at the beginning of the flight in the LT-BB plume (~0.5 nmol mol^{-1} and 1.90 µmol mol^{-1}), support this assumption of direct uplift to the UT outside of the squall line not affected by any wash-out processes prevalent inside the storm. However, interestingly rBC mass mixing ratios were low within the UT-BB plume (maximum <30 ng kg^{-1}, mean ~12 ng kg^{-1}) (see Figure 2e in HH2016). This observation indicates that perhaps other processes, e.g., sedimentation, possibly lowered the rBC mass mixing ratio in the UT-BB plume. Within the lofted plume on 12 June, water vapor measurements are available between 7 and 9 km altitude (82,500–82,860 s). The relative humidity was highly variable between ~10 and

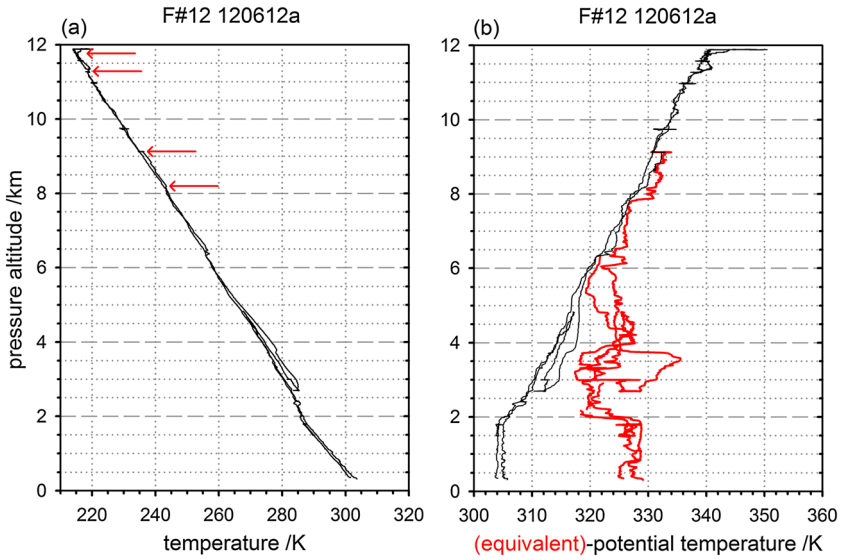

Figure 14. Vertical profiles of (a) temperature and (b) (equivalent)-potential temperature derived from Falcon measurements on 12 June 2012. The red arrows indicate two different tropopause levels at 11.2 and 11.8 km and a stratospheric intrusion between 8.2 and 9.1 km.

100%; however, most frequently values between 40% and 70% were measured and elevated H_2O mixing ratios in the range of ~0.3 g kg^{-1}, indicative of transport from lower levels. CO mixing ratios were elevated (100–180 nmol mol^{-1}) as expected in a plume generated from BB, but also ozone-rich stratospheric air masses (up to ~120 nmol mol^{-1}) mixed into the plume.

At ~85,000–86,000 s, as the aircraft left the anvil outflow at ~11 km to turn for the next higher flight level, the BB plume was not prominent anymore but O_3 mixing ratios were clearly enhanced (~140 nmol mol^{-1}) and CO mixing ratios decreased down to ~90 nmol mol^{-1} (Figure 13a). At the next higher level along the anvil edge (~12 km, ~87,000–87,500 s) the influence from the LMS was even more distinct with elevated O_3 mixing ratios over a horizontal distance of ~50 km with mixing ratios up to ~260 nmol mol^{-1} and CO mixing ratios as low as ~80 nmol mol^{-1}. In addition, NO and NO_x mixing ratios were still distinctly elevated during this time sequence inside the anvil outflow.

4.2.2. Discussion of 12 June 2012 Observations

A schematic of the major air mass transport pathways based on observations from 12 June 2012 is shown in Figure 15 (colored arrows). One side of the storm system was probed during stepwise ascent from 9.7 to 11.9 km altitude as indicated by the orange shaded area.

Within the center of the anvil outflow, low O_3 and elevated CO mixing ratios (70 and 120 nmol mol^{-1}, respectively) were observed indicating upward transport from lower altitudes below ~4 km, as illustrated by the green and yellow arrows near the storm core. In contrast, along the edges of the anvil outflow and at the highest flight level in the anvil outflow (~11.9 km, ~87,000–87,500 s) a clear mixing of elevated NO_x (mainly LNO_x) with O_3-rich stratospheric air masses (~260 nmol mol^{-1}) was observed. The highest flight level in the anvil outflow was located above the primary/secondary tropopause (~11.1/11.8 km) giving evidence of detrainment of LNO_x into the LMS.

Elevated O_3 mixing ratios were still measured down to ~8 km when the aircraft left the anvil outflow and started the steep descent for landing. Air masses of lower stratospheric origin not only mixed with the top and edges of the anvil outflow (straight red arrows) but also surrounded it as a stratospheric intrusion (curved red arrow). This latter air mass transport pathway is similar to the observations by *Pan et al.* [2014] as seen in O_3 lidar images. However, since lidar measurements are not available inside thick clouds such as thunderstorms, the direct downward injection of O_3-rich air masses into the anvil edges and upward injection of anvil-LNO_x into the LMS was not observed by *Pan et al.* [2014].

As in the previous flight described (Figure 7b), here we also observed that just outside and beneath the anvil outflow a lofted BB plume (curved yellow arrow in Figure 15) mixed with the stratospheric intrusion

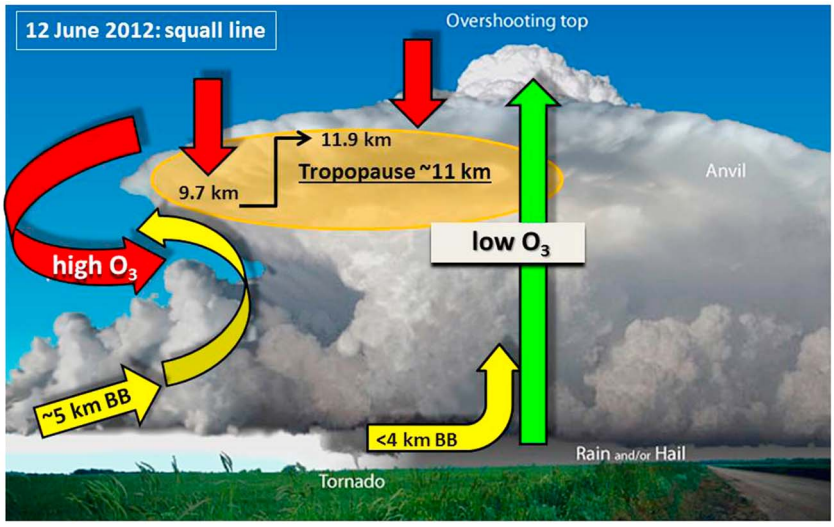

Figure 15. Schematic of an isolated, overshooting thunderstorm cell (credit: NOAA National Weather Service, http://www.srh.noaa.gov/jetstream/tstorms/tstrmtypes.htm). Superimposed are the major air mass transport pathways (colored arrows) observed during the Falcon flight on 12 June 2012 based on in situ trace gas measurements (CO and O_3) within the main vertical (and partly horizontal) extension of the anvil outflow from a squall line (orange shaded area). Emissions from wildfires (BB) and low O_3 mixing ratios are ingested into the overshooting squall line (yellow and green). As a response to the overshooting top, stratospheric air masses are transported downward along the boundaries of the anvil outflow (red). In addition, emissions from wildfires (BB, yellow) are ingested into towering cumulus along the flanking line of the squall line and mix with a stratospheric intrusion wrapped around the anvil outflow (red).

(~8–9.7 km). The O_3 mixing ratio in the lofted BB plume was much higher (twice as high) as observed before in the LT-BB plume at ~ 5 km (~60 nmol mol^{-1}), which excludes that the major O_3 enhancement was due to photochemical O_3 production.

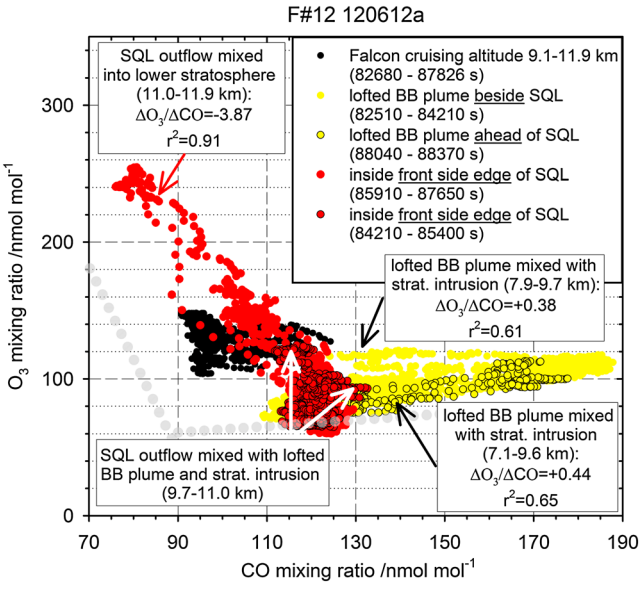

Figure 16. O_3-CO correlations during the Falcon flight on 12 June 2012 for the time period of the stepwise ascent below/inside the squall line (SQL) outflow at cruise altitudes 9.1–11.9 km and the descent to Salina. The correlations in the lofted BB plume and in the anvil outflow of the squall line are marked with yellow and red dots, respectively. The correlation in the free tropospheric and stratospheric background is marked with light gray dots.

To illustrate the strong influence of the squall line on the chemical composition in the UT/LS also the O_3-CO correlation in BB and LNO_x plumes was determined as shown in Figure 16. Just below and outside of the anvil outflow, the lofted BB plume (yellow dots) mixed with a stratospheric intrusion (~8–10 km), causing a positive regression slope ($\Delta O_3/\Delta CO$ ratio = +0.4) in the same range as observed in the 30 May case (Table 1). The anvil outflow at 9.7–11.0 km (red dots with black edges) was characterized by a mixture of O_3- and CO-rich air masses from the stratosphere and wildfires, indicating partly negative and partly positive O_3-CO correlations. The in-mixing partly took place along the boundaries of the anvil outflow, as indicated in Figures 13a and 15. Higher up within the anvil outflow (11.0–11.9 km), an increased in mixing of stratospheric air masses with altitude was observed (red dots without black edges), causing a negative O_3-CO correlation ($\Delta O_3/\Delta CO$ ratio = −3.9).

Table 3. Trace Gas and Particle (Here Only SP2) Measurements in the Anvil Outflow on 12 June 2012 (Separated According To Anvil Regions With Updrafts or Downdrafts and the Mean Over the Entire Anvil Outflow in Italic)[a]

DC3 Flight Number, Date, Flight a or b, Anvil Time	Pressure Altitude (km)	CO Mixing Ratio (nmol mol^{-1})	O_3 Mixing Ratio (nmol mol^{-1})	SO_2 Mixing Ratio (pmol mol^{-1})	CH_4 Mixing Ratio (nmol mol^{-1})	NO Mixing Ratio (nmol mol^{-1})	NO_x Mixing Ratio (nmol mol^{-1})	NO_y Mixing Ratio (nmol mol^{-1})	Ethane/Propane (pmol mol^{-1}/ pmol mol^{-1})	Benzene/Toluene (pmol mol^{-1}/ pmol mol^{-1})	rBC[b] Mass Mixing Ratio (ng kg^{-1})
F#12 120612a (84536–85260 s)	10.3 (9.7–11.0)	120 ± 3 (113/126)	73 ± 4 (65/85)	18 ± 13 (1/71)	1854 ± 3 (1849/1861)	0.6 ± 0.2 (0.2/1.1)	1.1 ± 0.5 (0.2/2.8)	-	-	-	-
upward											
F#12 120612a (84210–85400 s)	***10.4***	***↑121 ± 3***	***↓82 ± 14***	***↓25 ± 20***	***↑1854 ± 3***	***↑0.7 ± 0.5***	***↑1.2 ± 0.6***	-	-	-	-
Background (87939–87965 s)	**10.3 (10.2–10.4)**	**106 ± 1**	**120 ± 1**	**75 ± 20**	**1844 ± 1**	-	-	-	-	-	**17 ± 5**
F#12 120612a (85996–86999 s)	11.6 (11.0–11.9)	123 ± 2 (117/129)	72 ± 4 (60/80)	13 ± 9 (1/38)	1851 ± 3 (1845/1860)	1.5 ± 0.4 (0.8/3.1)	2.0 ± 0.5 (0.7/4.1)	-	1073/615 = 1.7[c]	16/64 = 0.3[d]	-
upward											
F#12 120612a (85910–87650 s)	***11.6***	***↑119 ± 10***	***↓91 ± 39***	***↓14 ± 10***	***↑1845 ± 16***	***↑1.5 ± 0.5***	***↑1.9 ± 0.6***	-	-	-	-
Background (87659–87832 s)	**11.3**	**97 ± 6**	**137 ± 8**	**38 ± 17**	**1833 ± 4**	**0.2 ± 0.1**	**0.5 ± 0.1**	-	-	-	**19 ± 10**

[a]Mean mixing ratios and standard deviations are given. Minimum and maximum mixing ratios are given in brackets. In addition, mean background mixing ratios outside the anvil outflow are given in bold. The arrows indicate if the anvil mixing ratios are higher (↑) or lower (↓) than the background mixing ratios.
[b]rBC = refractory black carbon.
[c]Compare to BL over Salina: 443/410 = 1.1.
[d]Compare to BL over Salina: 35/21 = 1.7.

In Table 3, trace species mixing ratios within the squall line is compared to the background. Elevated CO and low O_3 mixing ratios within the anvil outflow (~120 and ~80 nmol mol^{-1}) compared to the background (~100 and ~130 nmol mol^{-1}) indicate that the anvil outflow above ~10 km was surrounded by lower stratospheric air masses. SO_2 mixing ratios within the anvil outflow (~10–20 pmol mol^{-1}) were distinctly lower compared to the background (~40–80 pmol mol^{-1}) and the BL (>100 pmol mol^{-1}) suggesting efficient wash-out processes within the squall line (see also Figure 13d). In contrast, CH_4 mixing ratios were slightly elevated by ~10 nmol mol^{-1} within the anvil outflow compared to the background due to ingested wildfire emissions (see also Figure 13c). Within the anvil outflow peak NO (NO_x) mixing ratios, 3.1 (4.1) nmol mol^{-1}, were observed at 11.0 km. Enhanced anvil NO_x was present above the primary tropopause (11.1 km) indicating injection into the LMS. The presence of ingested wildfire emissions within the anvil outflow is also supported by the enhanced ethane and propane mixing ratios (1073 and 615 pmol mol^{-1}) compared to the BL (443 and 410 pmol mol^{-1}) and the background from the previous flight on 30 May (247 and 29 pmol mol^{-1}), see also Table 2. Unfortunately, no VOC background measurements were available from the flight on 12 June. Within the anvil outflow, the benzene/toluene ratio (=0.3) was distinctly lower compared to the BL (=1.7) and similar to background values (=0.2) observed on 30 May, indicating no pronounced influence from fresh anthropogenic emissions in the BL. In addition, on 12 June low rBC mass mixing ratios (<20 ng kg^{-1}) were observed in the background.

The results from this second thunderstorm case study, 12 June (Figure 15), support the findings from the first presented DC3 Falcon case from 30

May (Figures 7a and 7b): (1) emissions from wildfires (high in CO) are ingested into the thunderstorm near the cloud base, (2) the storm produces an overshooting top, possibly facilitated by the large-scale double(triple)-tropopause structure, (3) the overshooting top injects high amounts of BB emissions and LNO_x into the LMS in addition to low O_3 mixing ratios from the BL, (4a) as a dynamical response, O_3-rich air from the LMS is transported downward into the edges of the anvil outflow and (4b) surrounds the outflow like an umbrella (stratospheric intrusion), (5a) in addition, a rapid uplift of "less diluted" emissions from wildfires from the LT to the UT is frequently observed outside of thunderstorms, most likely transported upward in towering cumulus clouds along the storm's flanking line, (5b) this lofted BB plume mixes with the stratospheric intrusion surrounding the anvil outflow.

Several of these major air mass transport pathways (1–5) have by chance been observed in previous thunderstorm studies as described in section 1. However, in this study we report for the first time on observations in different types of thunderstorm systems during one field campaign supported by a unique variety of airborne and ground-based measurements. Furthermore, during DC3 the influence of smoke plumes and stratospheric air masses on the thunderstorm environment was much more pronounced than during previous U.S. thunderstorm field experiments. Wildfire emissions were useful tracers to construct a general picture of trace gas transport pathways within and nearby DC3 thunderstorms. Air mass pathways as (4a), (4b), (5a), and (5b) have rarely been observed and described before. However, they indicate a distinct influence of O_3-rich air masses from the LMS on the UT-O_3 composition inside and nearby thunderstorms besides the more well-known influence of low O_3 air transported from the BL. In the next subsection observations in aged thunderstorm outflow (~12–24 h) even more distinctly highlight the pronounced air mass exchange in the UT/LS region caused by thunderstorms.

4.3. The 8 June 2012: Aged MCS Outflow Over Colorado/Kansas

4.3.1. Observations on 8 June 2012

In the evening on 7 June, scattered severe convection developed over eastern Colorado that moved eastward and lasted until the next morning on 8 June. In the night the scattered convection and their anvils merged to a kind of MCS in the general sense (not as strict as defined by *Houze et al*. [1989]). On 8 June, the Falcon performed two flights to investigate the remnants of the MCS. The two flight patterns were similar, covering the major extension of the MCS remnants (~700 km wide) that spread across Kansas. In addition, the background air composition ahead and behind of the remnants was probed. The focus here is on the first Falcon flight around noon local time.

The GOES thermal-IR image for cloud top temperatures from the previous evening (http://catalog.eol.ucar.edu/cgi-bin/dc3_2012/ops/index) indicates that in agreement with the other two presented case studies the MCS cloud tops reached temperatures below −60°C. However, in this case the temperatures were slightly colder and extended over a larger area indicating that the main cloud deck reached even higher altitudes. During the mature stage of the MCS, an embedded storm cell close to Denver developed into a strong supercell with very high radar reflectivity (65–70 dBZ) (not shown), producing large hail and several tornadoes. At this time the average cloud top height in Figure 17a reached as high as ~13–14 km (higher, wider, and more homogeneous compared to the previous two cases in Figures 2b and 11). Between 18 and 00 UTC, the primary tropopause was located slightly lower at ~11–13 km according to the closest radiosoundings from Denver in eastern Colorado and Dodge City in southwestern Kansas (http://catalog.eol.ucar.edu/cgi-bin/dc3_2012/ops/index). These observations indicate that parts of the main cloud deck of the intense MCS very likely crossed the tropopause and mixed with air masses in the LMS.

During the flight the day after the mature MCS activity, not only thin cirrus clouds over western Kansas gave evidence of MCS cloud remnants (Figure 17b) but NCAR WRF forecasts of the column LNO_x tracer (8–16 km) were also used to determine the position of the MCS remnants and to guide the aircraft. The forecasts for 11 and 16 UTC (Figures 18a and 18b) predicted that the remnants (enhanced in LNO_x) spread eastward over Kansas and merged with less pronounced remnants of a second, weaker thunderstorm system over Texas and Oklahoma. At 16 UTC the major LNO_x plume from the aged MCS outflow is located west of Salina. The Falcon in situ observations of O_3 in this area indicate highly variable mixing ratios between ~60 and 150 nmol mol^{-1} in the UT (Figure 17b). Ahead (east) of the LNO_x plume a broad area with strongly enhanced O_3 mixing ratios (>150 nmol mol^{-1}) was observed which was caused by a pronounced stratospheric intrusion.

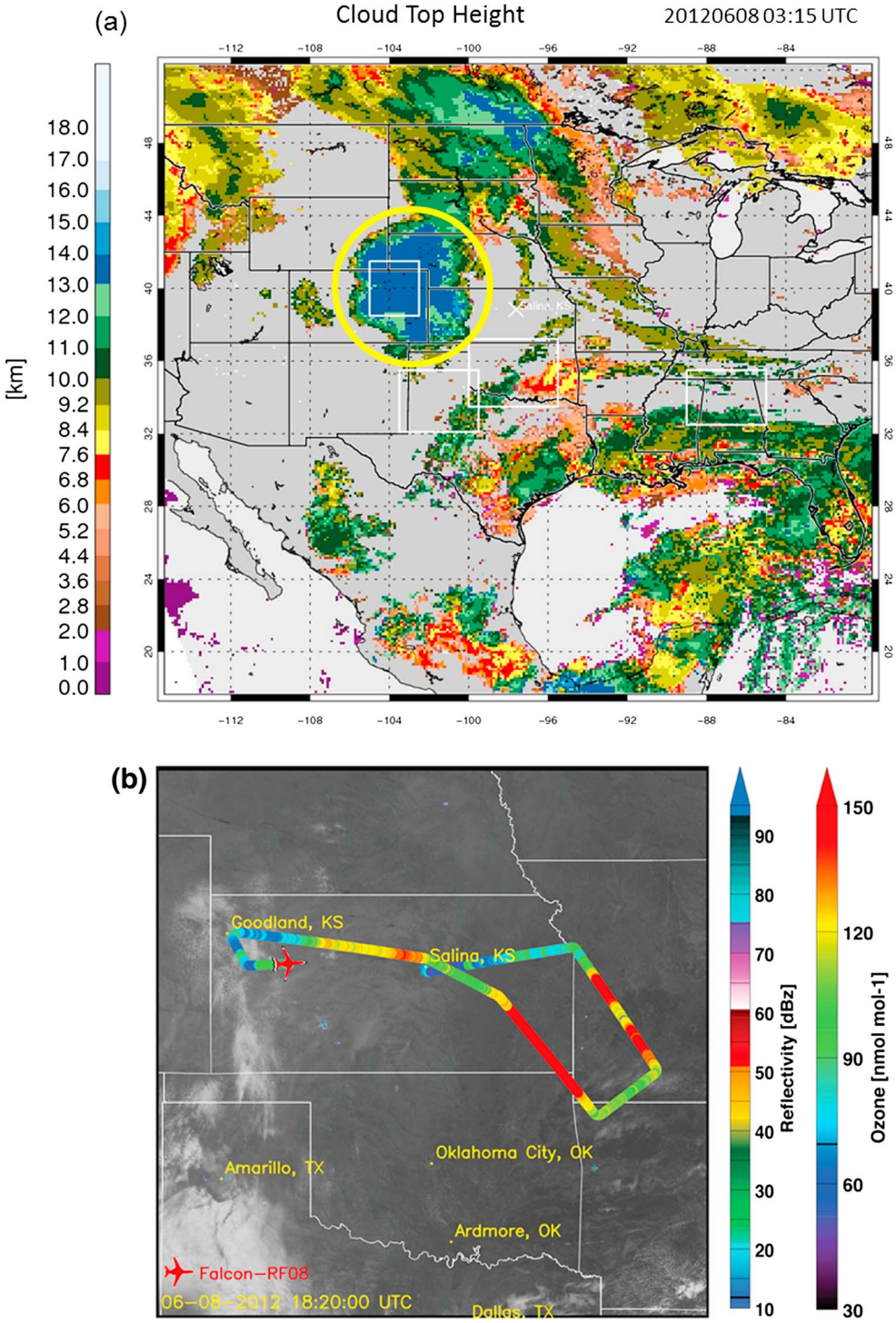

Figure 17. (a) Cloud top heights (in kilometer) derived from GOES data on 8 June 2012 at 03:15 UTC over the U.S. and Mexico (© NCAR/EOL). The yellow circle marks an extended MCS probed ~15 h later in a decaying stage over Kansas, Missouri and Arkansas (as shown in Figure 17b). The white squares mark the selected DC3 operation areas and the white cross the campaign base in Salina. (b) Flight tracks of the Falcon (red aircraft) on 8 June 2012 at 18:20 UTC. The flight tracks (color coded) are superimposed on a GOES IR satellite image (grey) and are color coded according to O_3 mixing ratios along the flight.

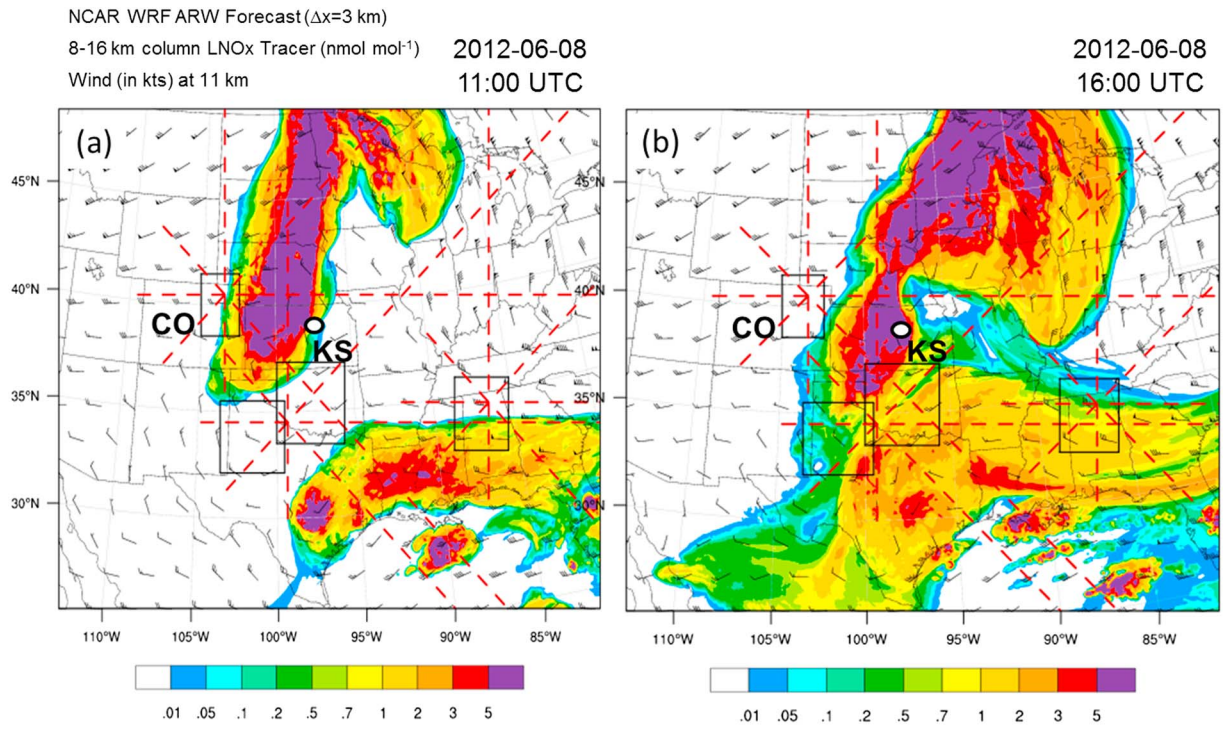

Figure 18. NCAR WRF Advanced Research Workshop forecast of 8–16 km column LNO_x tracer (color coded) and wind barbs at 11 km (black) for 8 June 2012 at (a) 11:00 and (b) 16:00 UTC. The DC3 campaign base (Salina, KS) is marked with a white black dot. The black squares mark the selected DC3 operation areas and the red dashed lines the available vertical cross sections for the LNO_x tracer.

Besides model forecasts and airborne measurements, satellite measurements of NO_2 from GOME-2 were also available for the region of interest (Figure 19). At 17 UTC, GOME-NO_2 data show that Kansas was entirely covered with enhanced tropospheric NO_2 vertical column densities up to $7–8 \times 10^{15}$ molecules cm^{-2}, most likely produced by lightning ~12–24 h earlier. Within the remnants of the MCS, the Falcon observed NO enhancements in the range of 0.5–1 nmol mol^{-1} between ~9 and 11.6 km altitude (~63,000–65,000 s and ~66,000–67,000 s) (Figures 20a and 20b). In addition, NO_y mixing ratios were clearly enhanced (~2–3 nmol mol^{-1}), and the low NO/NOy ratios (0.2–0.3) indicate that the LNO_x emissions were aged (Figures 20c and 20d). Furthermore, CH_4 mixing ratios reached up to 1.86 μmol mol^{-1}, and SO_2 mixing ratios were mostly $<$100 pmol mol^{-1}. Highly variable CO (~60–110 nmol mol^{-1}) and O_3 (~80–280 nmol mol^{-1}) mixing ratios were also observed within the aged outflow, most likely caused by dynamical processes. The maximum cruising altitude within the remnants of the MCS (11.6 km) coincide with the broad tropopause according to the vertical temperature profile from the Falcon (Figures 21a and 21b) and the 12 UTC radiosounding from Topeka in northeastern Kansas (http://catalog.eol.ucar.edu/cgi-bin/dc3_2012/ops/index).

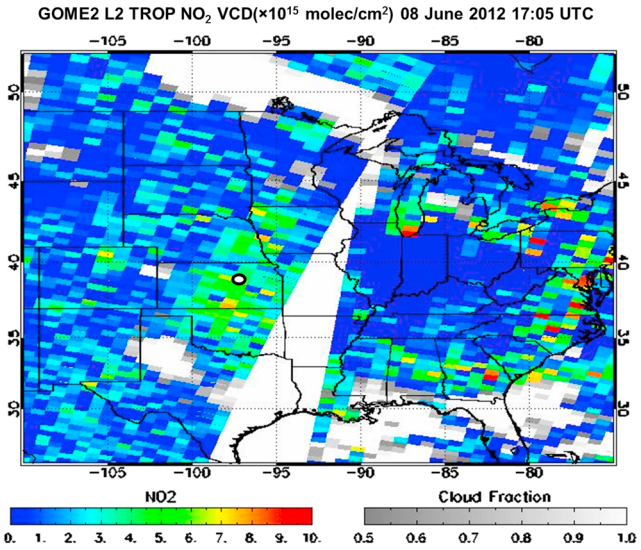

Figure 19. Tropospheric NO_2 vertical column densities measured by GOME-2 over the U.S. and Canada on 8 June 2012 at 17:05 UTC (color coded). The cloud fraction is superimposed in gray scales. The DC3 operation site (Salina, KS) is marked with a white black dot.

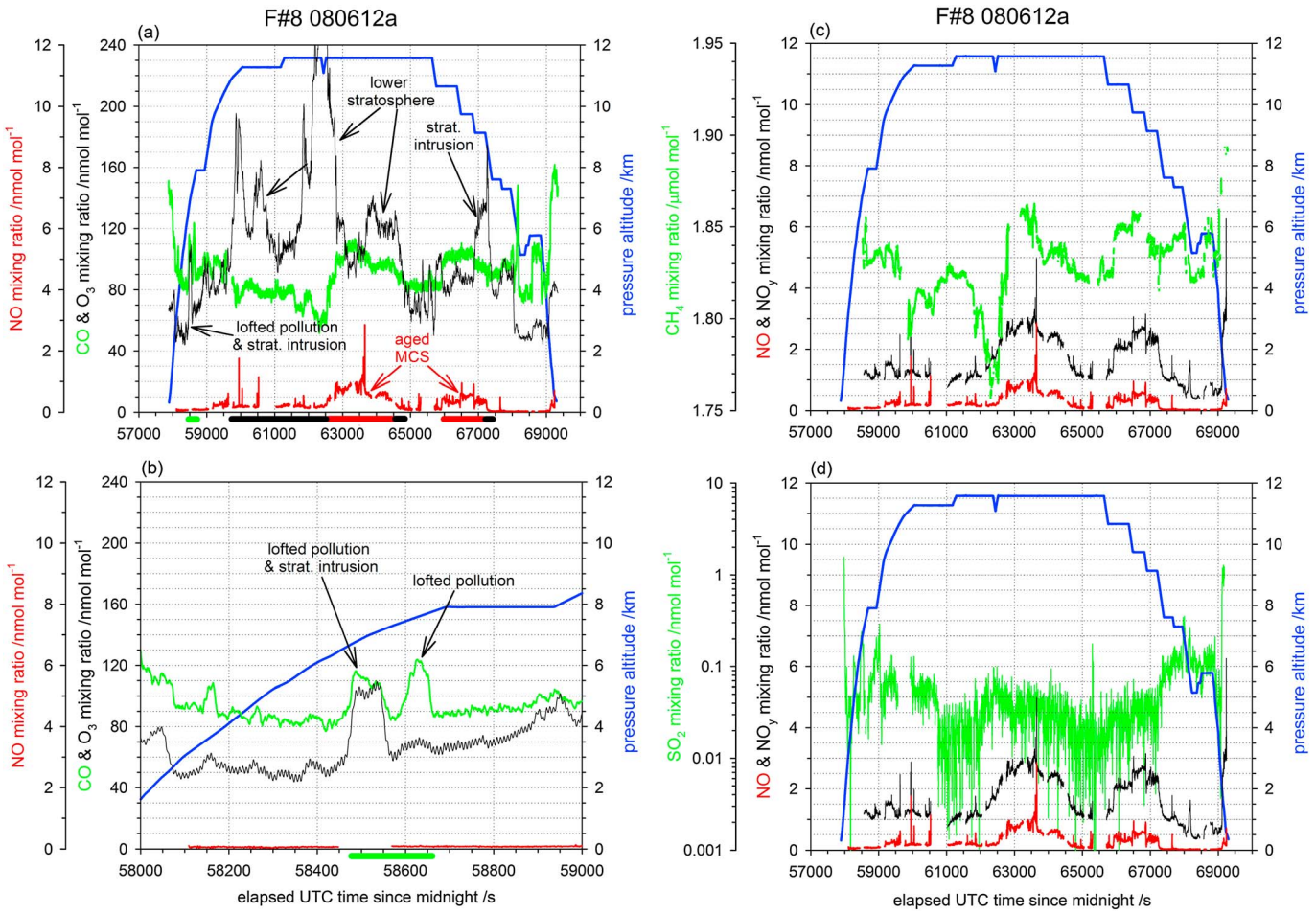

Figure 20. Time series of NO, NO_y, CO, O_3, SO_2, CH_4, and pressure altitude for the Falcon flight on 8 June 2012: (a, c, and d) complete flight and (b) selected time period from 58,000 to 59,000 s. Colored bars in Figures 20a and 20b indicate selected time sequences of the flight with different air masses: lofted pollution (green), stratospheric intrusion/lower stratosphere (black), and aged MCS outflow (red).

4.3.2. Discussion of 8 June 2012 Observations

Based on the Falcon trace gas time series in Figure 20a, major pathways for the most likely trace gas transport within and near the active MCS are illustrated in Figure 22. Almost the entire vertical and horizontal (E-W) extension of the MCS remnant was probed, as indicated by the orange shaded area (most complete probing compared to the two previous cases in Figures 7a and 15).

On 8 June, remnants of the MCS characterized by low O_3 and high CO mixing ratios (transport from below) were located near areas with elevated O_3 and low CO mixing ratios (transport from above) as indicated in the time series in Figure 20a and in Figure 22 by the different colored and directed arrows in the orange shaded area. The highly variable CO and O_3 mixing ratios observed at this altitude within the aged MCS outflow indicate a mixing and cross layering of lower stratospheric and upper tropospheric air masses in the broad tropopause transition zone.

In general, CO mixing ratios were not as enhanced as in the previously presented cases. The most likely BL pollution source in this case was anthropogenic pollution from Dallas and northern Texas, and not emissions from wildfires (results from FLEXPART analyses not shown here, see DC3 field catalog). As indicated in Figure 22, pollution was ingested near the cloud base of the MCS (yellow and green arrows) but was also present outside of the MCS and mixed with a stratospheric intrusion reaching as far downward as ~7 km (yellow and red curved arrows). The time sequence of the flight through the latter layer is presented in Figure 20b. Above this mixed polluted layer, a second polluted layer was observed, however, not mixed with stratospheric air masses. Low NO mixing ratios indicate that these two layers were most likely not processed inside the MCS.

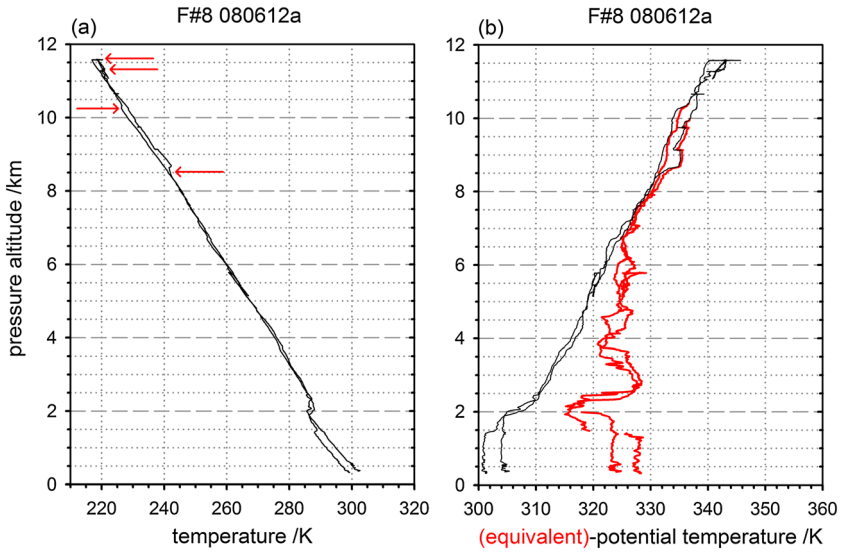

Figure 21. Vertical profiles of (a) temperature and (b) (equivalent)-potential temperature derived from Falcon measurements on 8 June 2012. The red arrows indicate two different tropopause levels at 11.2 and 11.6 km and stratospheric intrusions reaching down to 8.6 and 10.3 km, respectively.

On the other hand, elevated NO mixing ratios were observed within the entire aged MCS outflow probed between 8.8 and 11.6 km (outflow depth >2.8 km) (Figures 20a and 22). Near the upper boundary of the aged outflow (11.6 km), highly variable O_3 mixing ratios (up to 280 nmol mol^{-1}) coincided with elevated NO indicating mixing with lower stratospheric air masses (broad, red arrows in Figure 22). In addition, as indicated in Figure 20a (~67,000 s) the lower boundary of the aged outflow (~8–9 km) likely mixed with a stratospheric

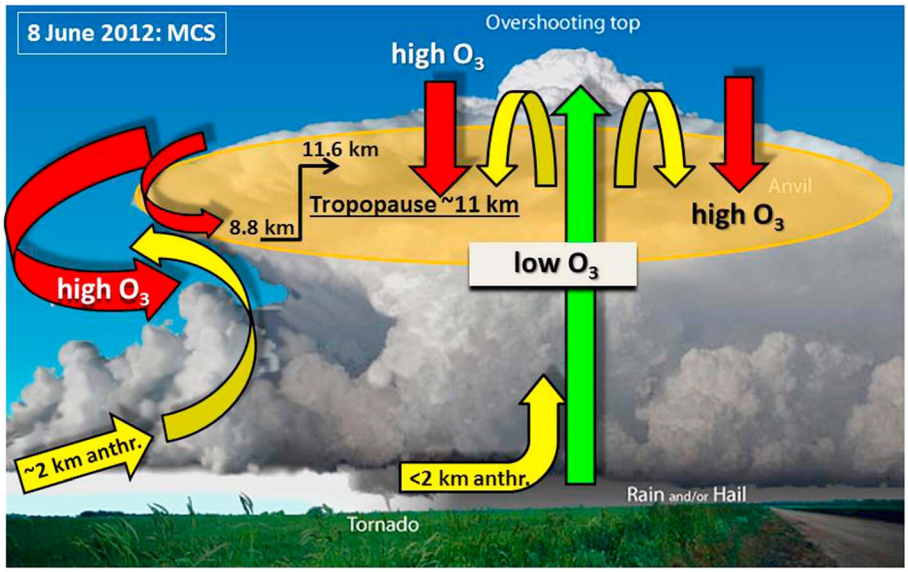

Figure 22. Schematic of an isolated, overshooting thunderstorm cell (credit: NOAA National Weather Service, http://www.srh.noaa.gov/jetstream/tstorms/tstrmtypes.htm). Superimposed are the major air mass transport pathways (colored arrows) observed during the Falcon flight on 8 June 2012 based on in situ trace gas measurements (CO and O_3) within the main vertical and horizontal extension of the anvil outflow from a MCS (orange shaded area). Anthropogenic emissions and low O_3 mixing ratios are ingested into the overshooting MCS (yellow and green). Strong updrafts and downdrafts within the storm redistribute the ingested pollution. As a response to the overshooting top, stratospheric air masses are transported downward into the anvil outflow (red). In addition, anthropogenic emissions (yellow) are ingested into towering cumulus along the flanking line of the overshooting MCS and mix with a stratospheric intrusion wrapped around the anvil outflow (red).

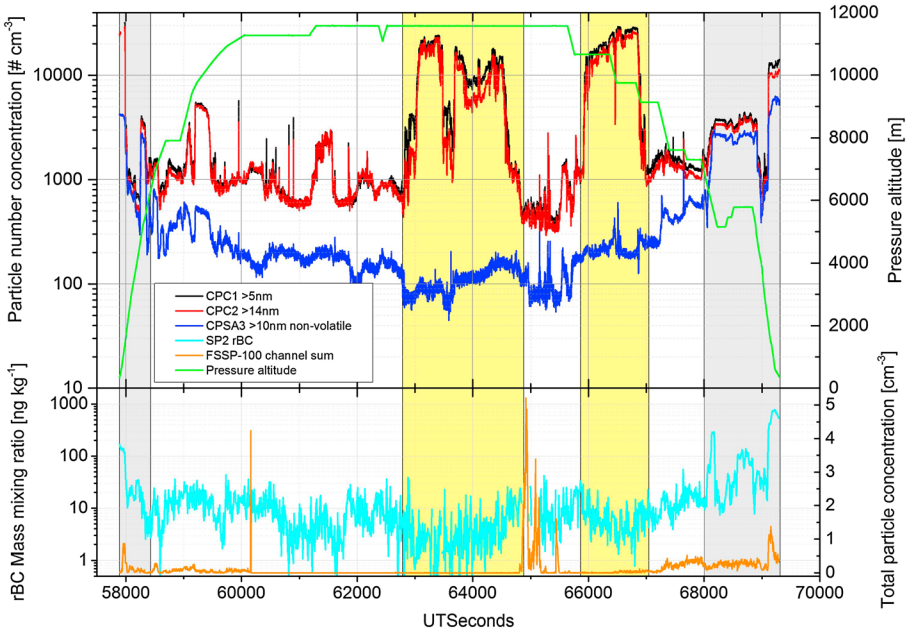

Figure 23. Time series of CPC (>5 nm, >14 nm, and nonvolatile >10 nm), rBC, FSSP-100, and pressure altitude for the Falcon flight on 8 June 2012. Shaded fields (in grey and yellow) indicate time sequences with enhanced concentration of particles >5 nm and >14 nm.

intrusion (up to 170 nmol mol^{-1}) wrapped around the outflow (red curved arrow in Figure 22). In agreement, the vertical temperature profiles indicate an inversion layer at 8.6 km (Figures 21a and 21b).

During the flight on 8 June the exchange of tropospheric and stratospheric air masses in the aged MCS outflow region was not the only striking process but also the strong influence of the MCS on the particle concentration in the UT/LS region. In Figure 23 time series of a variety of particle concentrations (condensation particle counter (CPC), rBC, and Forward Scattering Spectrometer Probe (FSSP)-100) are shown for the first flight on 8 June. Within the aged MCS outflow at 11.6 km and during the descent through the outflow (both areas highlighted in yellow), the FSSP-100 concentrations are generally low indicating almost cloud free conditions. In addition, the rBC mass mixing ratios are rather low (<10 ng kg^{-1}), most likely due to wash-out processes. In contrast, high numbers of condensation nuclei CPC >5 nm and >14 nm are present (up to 20,000–30,000 particles STP cm^{-3}). These concentrations partly exceed the concentrations observed in the BL and are most likely produced in situ (by dynamical effects and from precursors as SO_2 and VOCs, see below). The measurements in the aged outflow indicate that new ultrafine particles are formed, since CPC >5 nm partly exceeds the value for CPC >14 nm. The low concentration of nonvolatile particles (~100 particles STP cm^{-3}) supports the suggestion of in situ production prevailing over the upward particle transport from the BL. Of all Falcon DC3-flights in the vicinity of thunderstorms, this is the only flight that shows clear evidence of new particle formation.

Next the $\Delta O_3/\Delta CO$ ratio in the lofted pollution layers (~7–8 km) and in the aged MCS outflow (~9–12 km) mentioned above is discussed for the Falcon flight on 8 June. The influence of the stratospheric intrusion on the polluted layers probed during the ascent from Salina is shown in Figure 24a (see also Figures 20b and 22). The $\Delta O_3/\Delta CO$ ratio was enhanced (+1.4) in the lower pollution layer located at 6.6–7.2 km due to mixing with a stratospheric intrusion. Within the core of this layer a negative $\Delta O_3/\Delta CO$ ratio (−0.4) was observed, as typical for stratospheric influenced air masses. In contrast, the second lofted pollution layer located above the first one at 7.4–7.9 km was not impacted by the stratospheric intrusion. The observed $\Delta O_3/\Delta CO$ ratio (+0.1) in this plume agrees with observations in lofted BB plumes (<7 km) not mixed with stratospheric air masses and suggests only a weak photochemical O_3 production, ~5–10 nmol mol^{-1} (see Figure 24a and Table 1). Within the aged MCS outflow (~63,000–65,000 s and ~66,000–67,000 s) in Figure 20a, distinct negative $\Delta O_3/\Delta CO$ ratios (−3.8 and −3.4, respectively) were observed in the lower boundary (8.8–10.7 km), as well as in the upper boundary (at 11.6 km) of the aged outflow (Figure 24b).

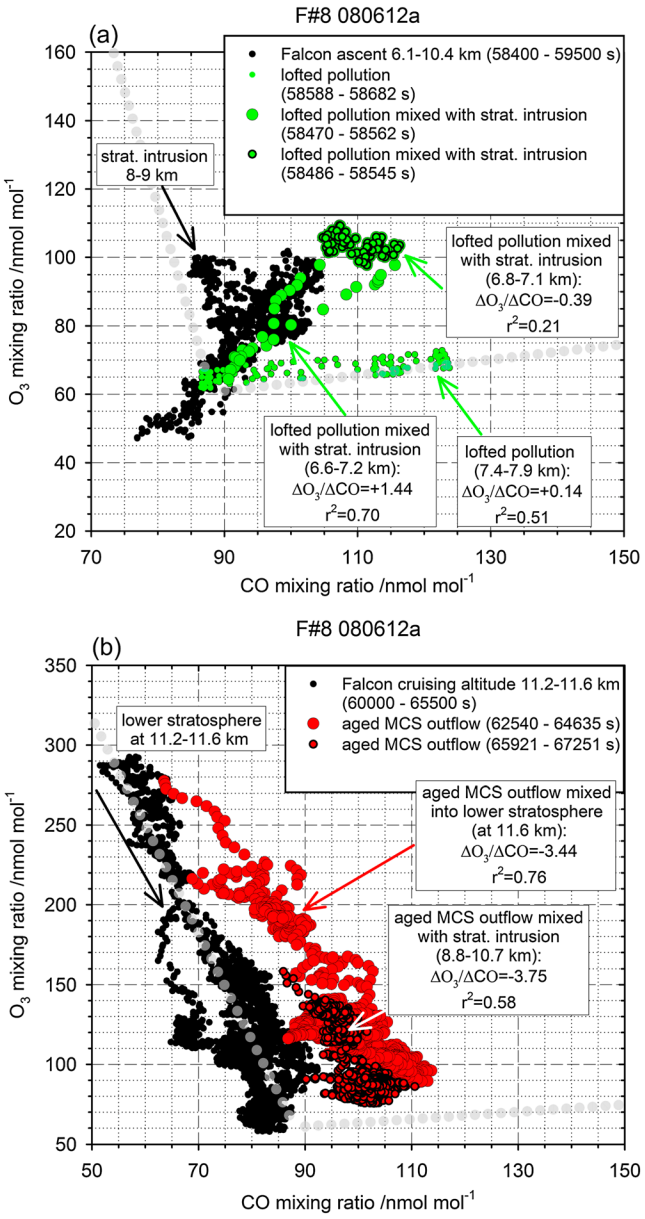

Figure 24. (a) O_3-CO correlations during the Falcon flight on 8 June 2012 for the time period of the ascent from Salina. The correlations in lofted pollution plumes are marked with green dots. (b) O_3-CO correlations during the Falcon flight on 8 June 2012 for the time period of the cruising at 11.2–11.6 km and the descent to Salina. The correlations within the anvil outflow of the MCS are marked with red dots. The correlation in the free tropospheric and stratospheric background is marked with light gray dots.

Here the mixing of the aged MCS outflow with air masses from the LMS was prominent throughout the entire anvil outflow region, as illustrated in Figure 22 in the orange shaded area by the different colored arrows.

A summary of the chemical composition ratio observed in the aged MCS outflow on 8 June compared to the background is given in Table 4. The day after the major convective activity CO mixing ratios at ~10–12 km altitude were only slightly enhanced by ~10 nmol mol^{-1}. In contrast, O_3 mixing ratios were distinctly enhanced compared to the background by ~20–50 nmol mol^{-1} on average over a wide horizontal distance of up to ~200 km, indicating a distinct downward mixing of O_3-rich air masses from the LMS and simultaneously in-mixing of tropospheric air masses (rich in CO and low in O_3) into the LMS. CH_4 mixing ratios were slightly enhanced (up to 1.85 μmol mol^{-1}) compared to the background due to upward transport of pollution. As in the previous cases, SO_2 mixing ratios were low (~30 pmol mol^{-1}) within the aged outflow due to efficient wash-out effects. In agreement to our observations, high scavenging efficiencies in the range of 80% have been observed by *Yang et al.* [2015] in other DC3 thunderstorms on 29 and 30 May 2012. In addition, H_2SO_4 was most likely formed from SO_2 and acted as a precursor for the formation of new particles (Figure 23).

On 8 June, the influence from LNO_x was still observable in the aged MCS outflow with mean NO and NO_y mixing ratios in the range of 0.5 and 2.5 nmol mol^{-1}, respectively, both well enhanced above typical background values (Table 4). In addition, the high ethane and propane mixing ratios (>1200 pmol mol^{-1}) and benzene/toluene ratio (1.0) indicate a prominent influence of anthropogenic pollution transported upward from the BL to the anvil outflow region. The rBC mass mixing ratio was low (5–7 ng kg^{-1}) within the aged MCS outflow compared to the background (11–16 ng kg^{-1}), most likely influenced by efficient wash-out processes. In comparison, the concentration of condensation nuclei >5 nm and >14 nm was much larger in the aged outflow (~10,000–30,000 particles STP cm^{-3}) compared to the background (~500–1000 particles STP cm^{-3}) as a result of new particle formation.

The last presented case study from 8 June clearly shows that tropospheric and stratospheric air masses are efficiently mixed in the aged MCS outflow region (Figure 22). The irreversible in-mixing of UT air masses with

Table 4. Trace Gas and Particle (Here Only SP2) Measurements in the Anvil Outflow on 8 June 2012 (Separated According To Anvil Regions With Aged Outflow and the Mean Over the Entire Anvil Outflow in Italic)[a]

DC3 Flight Number, Date, Flight a or b, Anvil Time	Pressure Altitude (km)	CO Mixing Ratio (nmol mol^{-1})	O_3 Mixing Ratio (nmol mol^{-1})	SO_2 Mixing Ratio (pmol mol^{-1})	CH_4 Mixing Ratio (nmol mol^{-1})	NO Mixing Ratio (nmol mol^{-1})	NO_x Mixing Ratio (nmol mol^{-1})	NO_y Mixing Ratio (nmol mol^{-1})	Ethane/Propane (pmol mol^{-1} /pmol mol^{-1})	Benzene/Toluene (pmol mol^{-1}/ pmol mol^{-1}	rBC[b] Mass Mixing Ratio (ng kg^{-1})
F#8 080612a (62540–64635 s) aged outflow	*11.6*	*↑98 ± 8 (64/114)*	*↑127 ± 30 (88/278)*	*↑35 ± 15 (1/94)*	*↑1839 ± 15 (1773/1863)*	*↑0.7 ± 0.2 (0.1/2.9)*	-	*↑2.5 ± 0.3 (1.5/5.0)*	*1930/1357 = 1.4*	*26/86 = 0.3*	*↓5 ± 5 (0/39)*
Background[c] (64636–65638 s)	**11.6**	**84 ± 3**	**77 ± 13**	**20 ± 20**	**1825 ± 4**	**0.1 ± 0.06**	**-**	**1.2 ± 0.1**	**478/124 = 3.9**	**6/91 = 0.1**	**11 ± 8**
F#8 080612a (65921–67251 s) aged outflow	*9.9*	*100 ± 4 (86/111)*	*↑97 ± 20 (76/158)*	*↓32 ± 13 (1/72)*	*↑1848 ± 7 (1818/1859)*	*↑0.4 ± 0.1 (0.1/1.0)*	-	*↑2.3 ± 0.3 (1.6/3.2)*	*1737/1243 = 1.4*	*25/25 = 1.0*	*↓7 ± 4 (1/23)*
Background 3(59286–59366 s)	**9.8-10.0**	**99 ± 2**	**81 ± 2**	**76 ± 16**	**1838 ± 1**	**0.2 ± 0.01**	**-**	**1.5 ± 0.03**	**-**	**-**	**16 ± 7**

[a]Mean mixing ratios and standard deviations are given. Minimum and maximum mixing ratios are given in brackets. In addition, mean background mixing ratios outside the anvil outflow are given in bold. The arrows indicate if the anvil mixing ratios are higher (↑) or lower (↓) than the background mixing ratios.
[b]rBC = refractory black carbon.
[c]Background: both CO and O_3 mixing ratios are low indicating a mixture of tropospheric and stratospheric air masses.

O_3-rich air masses in the LMS is prominent at least up to 11.6 km altitude. Here elevated NO mixing ratios (on average ~0.5–1 nmol mol^{-1}) from LNO_x was observed to coincide with stratospheric O_3 mixing ratios up to 278 nmol mol^{-1}. In contrast, the cause for the elevated O_3 mixing ratios observed within the aged anvil outflow in the UT is most likely in-mixing from the LMS. Any pronounced contribution from photochemical O_3 production is not obvious in our observations within the aged thunderstorm outflow after 12–24 h, due to the dominance of the dynamical contribution from the LMS. The observed O_3 enhancement (~20–50 nmol mol^{-1} on average) in the UT is far too high and the $\Delta O_3/\Delta CO$ ratios (−3.4/−3.8) are far too low to result from photochemical production alone (~5–20 nmol mol^{-1} d^{-1} and a positive correlation expected, see section 1). Perhaps, the duration with daylight (~6 h) was too short to produce significant O_3 amounts. From our measurements it is, however, not possible to investigate if a smaller contribution to the observed O_3 enhancement was generated by photochemical O_3 production, since HO_x measurements were not available on the Falcon. A MCS case study including HO_x measurements on the DC8 during DC3 is in preparation by C. Cantrell (private communication, 2015).

5. Discussion of Observed Ozone Enhancements Within Thunderstorms

In section 1, present knowledge on major processes responsible for O_3 enhancements in thunderstorm outflow were summarized, i.e., *photochemical O_3 production and stratospheric downward mixing*. The presented case studies from DC3 indicate that the latter process was most dominant in the central U.S. thunderstorms investigated by the Falcon during May–June 2012. This result is not surprising given that the sampling was conducted in convection that had been exposed to less than ~6 h of sunlight, likely not long enough for much O_3 production to occur.

A further mechanism responsible for O_3 enhancements within thunderstorms has been discussed by *Zahn et al.* [2002]. During a number of commercial "Civil Aircraft for Regular Investigation of the Atmosphere Based on an Instrument Container" (CARIBIC) flights, "ozone-rich transients" (up to ~2000 nmol mol^{-1}) over a horizontal distance of 5–80 km were occasionally observed

in the vicinity of deep convection, which were attributed to "measurement artifacts" (trigger electrical "corona" discharges on the aircraft fuselage or sampling inlets). During DC3, we observed this type of brief O_3 enhancements (without accompanying CO signature) due to a triggered flash during one Falcon flight on 6 June 2012 (see Falcon flight reports: http://catalog.eol.ucar.edu/dc3_2012/missions/missions.html).

In the past, ozone-rich transients have also frequently been observed during "Measurements of Ozone and Water Vapor by In-service Aircraft" (MOZAIC) flights over the equatorial Atlantic Ocean, as reported by *Suhre et al.* [1997]. About one third of all flights showed signatures of enhanced O_3 (~100–500 nmol mol^{-1}, also 5–80 km wide at 10–12 km), occasionally coinciding with enhanced water vapor, turbulence, and wind changes when the aircraft passed under a thunderstorm anvil at a distance of at least 15–30 km from convective towers. *Suhre et al.* [1997] suggested that a stratospheric influence, "the downward turbulent transfer through the tropopause caused by convection," was the main cause for the observed O_3 enhancements. When precipitation streaks loaded with ice particles fall from an overshooting anvil, water vapor and O_3-rich air may be transported downward through the tropopause region into the UT. The continuous evaporative cooling of the ice particles causes a rapidly downward moving air mass and a reduction of its potential temperature. This microphysical process would produce "cold" downdrafts. However, detailed radar measurements in squall line systems by *Biggerstaff and Houze* [1993] have shown that the upper level downdrafts are "warm" and dynamically induced compared to the microphysically forced cold downdrafts at lower levels between the surface and ~5 km. They proposed that the upper level downdrafts were caused by gravity waves as a result of the strong convective updrafts. Model simulations by *Wang* [2003] have also shown that gravity wave breaking at the top of deep convective systems in the midlatitudes may cause an air mass exchange between stratosphere and troposphere. *We believe that such a dynamical mechanism, as suggested by, e.g., Biggerstaff and Houze* [1993] *and Wang* [2003]*, may explain the O_3 enhancements in the vicinity of thunderstorms that we observed during DC3.* Also, coexisting signatures in other trace gases during DC3, e.g., CO and CH_4, support the presence of a dynamical mechanism. This type of downdraft structure has commonly been observed by radar measurements in supercells in the past [*Payne et al.*, 2010] and is similar to the upper level rear flank downdraft in the *Lemon and Doswell* [1979] conceptual model of supercell storms.

Compared to most other studies, where O_3 enhancements from thunderstorms were more or less accidentally observed during commercial flights (e.g., CARIBIC and MOZAIC) or during single research flights (section 1), the gain of the DC3 experiment was the selective targeting of different thunderstorm types in different developing stages over a wide area over the central U.S. supported by a variety of airborne in situ trace species measurements, dense ground-based networks of radar and lightning detection systems, and satellite data. Thus, the measured O_3 enhancements from thunderstorms could more easily be assigned to certain regions of the thunderstorms and its outflow and were found to extend over wide areas (~20–200 km) and to coexist with pronounced gradients in other trace gases.

To our knowledge, the study presented here is the first one of its kind where a general picture of the major transport paths within and in the vicinity of the central U.S. thunderstorms is obtained as schematics (Figures 7, 15, and 22) based on such a comprehensive data set: (1) *The wrapping of stratospheric air around the anvil outflow* in our schematic pictures based on Falcon measurements is also confirmed by O_3 lidar measurements on board the NASA-DC8 aircraft during DC3 [*Pan et al.*, 2014] and has been suggested to result from radiated gravity waves initiated when the strong convective updrafts deform the tropopause upward [*Hitchman et al.*, 2004]. (2) *The direct injection of O_3-rich stratospheric air masses into the UT anvil outflow* in our schematic pictures based on Falcon measurements has only rarely been observed in the past. Our case study from 30 May indicates that the vigorous nature of a supercell and MCC thunderstorm may connect polluted layers located in the LT with the ~10 km distant LMS, thereby reversing the chemical composition ratio in the UT/LS region. Until now our present knowledge about cross-tropopause tracer transport was mainly based on results from model studies with, e.g., WRF and cloud-resolving models. These studies indicate that overshooting tops have the potential to inject large amount of LT air into the LMS [e.g., *Mullendore et al.*, 2005; *Homeyer et al.*, 2014] and in the opposite direction [e.g., *Frey et al.*, 2015].

The three case studies we presented herein and in HH2016 give enough evidence to propose that "*in May–June in the UT/LS region over the central U.S. a pronounced exchange of tropospheric and lowermost stratospheric air masses is present which is influenced by the frequent occurrence of intense thunderstorms.*" One main question is if the observed O_3 enhancements in the aged anvil outflow during DC3 significantly contribute to

maintain the recurring UT-O_3 maximum as observed by *Li et al*. [2005] in a stationary anticyclone centered over the southeastern U.S. later in summer during the NA monsoon. Until recently, the downward mixing of O_3 rich air from the stratosphere and ozone precursors (NO_x and VOCs) transported upward from the BL by convection were found to only play a minor role and O_3 production by aged LNO_x was found to play the dominant role in this anticyclone [*Choi et al*., 2005; *Cooper et al*., 2006, 2007; *Choi et al*., 2008; *Cooper et al*., 2009; *Zhao et al*., 2009; *Allen et al*., 2010, 2012]. In a sensitivity test, *Cooper et al*. [2007] increased global LNO_x emissions from 2.2 Tg a^{-1} to 6.6 Tg a^{-1} in their European Centre/Hamburg 5 (ECHAM5)/MESSy1 chemistry general circulation model during the 2006 summer monsoon and achieved a better agreement between ozone measurements and model results supporting the importance of LNO_x for O_3 production in the stationary anticyclone. However, for some regions (e.g., at 10–11 km above Huntsville, Alabama) the discrepancies between ozone observations and model results were still large. *Cooper et al*. [2007] suggested that the presence of aged ozone-rich stratospheric air masses in the UT region could contribute to this discrepancy; however, the spatial model resolutions implemented in the UT/LS region was too coarse to study this transport in detail. Further simulations with global models over NA in summer have shown large discrepancies in quantifying UT-O_3 and $-NO_x$ produced by lightning compared to observations [*Pfister et al*., 2008; *Hudman et al*., 2009; *Jourdain et al*., 2010]. *Wang et al*. [2013] pointed out that present model predictions for UT-O_3 over NA are generally too low and still differ by ~20–25 nmol mol^{-1} compared to measurements with ozonesondes. First recent CTM results by *Tang et al*. [2011] suggest that the cause of the persistent ozone maximum observed in summer over northern midlatitude continents (e.g., over the central U.S.) is a deep convective stratosphere-troposphere exchange flux. Only a small number of all convective events penetrate into the LMS, but these events may induce a pronounced downward O_3-flux as reaction of the tropopause upward deformation [*Tang and Prather*, 2010]. In addition, high-resolved simulations of the meteorology and chemistry with the WRF-Chem model by *Barth et al*. [2012] and *Homeyer et al*. [2014] suggest that the entrainment of O_3-rich air from the stratosphere may play a major role for the UT-O_3 maximum observed during the NA monsoon. Our measurements in a number of thunderstorms during DC3 support these more recent results and give evidence of a more pronounced influence from the stratosphere on the convective outflow in specific regions, such as the central U.S., at least during specific periods (May–June). Later during the NA monsoon (June–August) the tropopause height is increasing, and most convective systems are less severe which would most likely cause a less pronounced O_3 contribution from the stratosphere and a larger contribution from LNO_x as suggested by *Cooper et al*. [2007].

6. Summary and Conclusions

A unique data set on chemistry and dynamics within and in the vicinity of the central U.S. thunderstorms sampled during the DC3 field experiment in summer 2012 was presented. We focused on in situ trace species measurements (CO, O_3, SO_2, CH_4, NO, NO_x, NO_y, VOC, CN, and black carbon) carried out by the German DLR-Falcon aircraft in fresh (<12 h) and aged (~12–24 h) anvil outflow (~9–12 km altitude) from different thunderstorm types (MCS, MCC, supercells, and squall lines) over Oklahoma, Texas, Colorado, and Kansas. A combination of trace gas time series and correlations (O_3-CO), radar, lightning, and satellite information, as well as model results from WRF and FLEXPART, was used to analyze and design schematics of major trace gas transport pathways within and in the vicinity of the probed thunderstorms to study the impact of thunderstorms on the UT/LS O_3 composition. On most thunderstorm days, dense smoke plumes from huge wildfires in New Mexico and Colorado were also present. These wildfire emissions in the vicinity of the probed thunderstorms, characterized by pronounced trace gas gradients, were useful tracers to construct a general picture of trace gas transport pathways within and nearby thunderstorms.

The analyses indicate that the investigated thunderstorms influenced the chemical composition ratio of the UT/LS region over the central U.S. significantly in accordance with first findings presented in HH2016. A distinct redistribution and production of trace gases, especially CO, O_3 and NO_x, was observed in the UT/LS region. Within and in the vicinity of thunderstorms, O_3-poor (CO-rich) air from the LT was transported upward to the UT, as known from previous thunderstorm studies. However, compared to past thunderstorm campaigns [see, e.g., *Schumann and Huntrieser*, 2007, Table 10; *Huntrieser et al*., 1998, 2002, 2008, 2009, 2011], the frequency and intensity of events with O_3-poor (CO-rich) air penetrating the tropopause into the LMS, and simultaneously O_3-rich air transported downward from the LMS to the UT, was especially high during

DC3. On a regular basis, the probed DC3 storms developed overshooting tops promoting the stratosphere-troposphere exchange of air masses. Furthermore, the results from three DC3 case studies gave sufficient evidence that the in-mixing of O_3-rich air masses from the LMS (and not photochemical O_3 production) was the major source of elevated O_3 mixing ratios observed within and in the vicinity of fresh and aged anvil outflow:

1. On the Falcon flight on 30 May 2012 in the center of the fresh anvil outflow from an overshooting supercell, where also the highest lightning NO mixing ratios were observed (8.6 nmol mol^{-1}), O_3 mixing ratios as low as ~70 nmol mol^{-1} were observed at ~9 km altitude, indicating upward transport from lower levels (LT). In contrast, along the boundaries of the anvil outflow a mixture of O_3-rich air masses (up to ~140 nmol mol^{-1}) from the LMS and CO-rich air masses (up to ~160 nmol mol^{-1}) from BB emissions (Whitewater-Baldy Fire) was observed. In addition, on 30 May, we observed that the fresh anvil outflow from a nearby overshooting MCC was surrounded by a stratospheric intrusion similar to the observations by *Pan et al*. [2014]; in our case lofted BB emissions (CO ~120 nmol mol^{-1}) located below the MCC outflow (~8–10.5 km) mixed with O_3-rich air masses from the LMS (O_3 ~ 150 nmol mol^{-1}). In summary, our observations indicate that the major impact on the UT/LS O_3 composition within and in the vicinity of the investigated supercell and MCC outflow must have been caused by dynamical (and not photochemical) processes, because the observed trace gas gradients have larger amplitudes than expected from photochemical processes only. In addition, this was further supported by measurements of the vertical velocity by aircraft and from multi-Doppler radar analyses.
2. On the Falcon flight on 12 June 2012 in the fresh outflow from a squall line, low O_3 mixing ratios in the range of 70 nmol mol^{-1} were observed throughout the center of the outflow layer between ~9.5 and 12 km altitude in conjunction with elevated CO mixing ratios in the range of 120 nmol mol^{-1} from BB emissions (High Park Fire) transported upward from the LT. At the highest flight level (~12 km), both air masses of LT origin as well as LMS origin (~260 and ~80 nmol mol^{-1} O_3 and CO, respectively) were observed next to each other in the anvil outflow in conjunction with lightning-produced NO in the range of 1–3 nmol mol^{-1}. In addition, a stratospheric intrusion was wrapped around the overshooting anvil outflow and reached down to ~9 km with O_3 mixing ratios as high as ~120 nmol mol^{-1}. Just below the anvil outflow (~8–9.5 km), lofted BB emissions (CO ~180 nmol mol^{-1}) mixed with the stratospheric intrusion.
3. On the Falcon flight on 8 June 2012 in the aged outflow (~12–24 h) from scattered severe convection organized to a MCS, anthropogenic pollution with CO mixing ratios exceeding ~100 nmol mol^{-1} was transported upward from the LT and mixed with O_3-rich air masses (>200 nmol mol^{-1}) at ~11.5 km altitude. Observed O_3 enhancements (~20–50 nmol mol^{-1} on average) were far too high and $\Delta O_3/\Delta CO$ ratios (down to −3.8) far too low to result from photochemical production (~5–20 nmol mol^{-1} d^{-1} and a positive correlation expected) and instead the in-mixing of O_3-rich stratospheric air masses was suggested to cause these enhancements. In addition, enhanced NO mixing ratios produced by lightning (~0.5–1 nmol mol^{-1}) mixed with these O_3-rich air masses. Furthermore, a stratospheric intrusion with O_3 mixing ratios as high as ~170 nmol mol^{-1} was wrapped around the lower boundary of the MCS outflow and reached down to 8–9 km altitude. The highly variable CO and O_3 mixing ratios observed within the aged MCS outflow were most likely caused by mixing and layering of lower stratospheric and upper tropospheric air masses. Of all Falcon DC3-flights in the vicinity of thunderstorms, this is the only flight that shows clear evidence of new particle formation. Results from past field experiments have shown that new particle formation is a common process observed in the vicinity of deep convection due to convective lifting and formation from precursors such as SO_2 [*Thornton et al*., 1997; *de Reus et al*., 1999; *Wang et al*., 2000; *Huntrieser et al*., 2002].

Our findings from the above mentioned case studies can be summarized as follows (see also schematics of major trace gas pathways in Figures 7, 15, and 22): a rapid uplift of less diluted emissions from wildfires (high in CO, SO_2, and rBC) from the LT to the UT is frequently observed in the vicinity of thunderstorms, most likely transported upward in towering cumulus clouds along the storm's flanking line; emissions from wildfires are also ingested into the thunderstorm near the cloud base; DC3 thunderstorms frequently produce an overshooting top, possibly facilitated by the large-scale double (triple)-tropopause structure; the overshooting top injects high amounts of BB emissions (mainly CO) and LNO_x into the LMS in addition to low O_3 mixing ratios from the LT; as a dynamical response (most likely gravity waves), O_3-rich air from the lowermost stratosphere is transported downward directly into the anvil outflow and in addition surrounds the outflow like an

umbrella (stratospheric intrusion); and the lofted BB plume mixes with the stratospheric intrusion surrounding the anvil outflow.

In comparison to the described, pronounced trace gas exchange in the UT/LS region initiated by dynamical processes, no clear signatures of photochemical O_3 production were observed within the anvil outflow probed during the presented DC3 Falcon flights. The exposure to daylight (<6 h) was probably too short. We expect that sufficient UT-HO_x is available for the production, but the observed production rate (<10 nmol mol^{-1}) in the lofted BB and anthropogenic plumes is negligible in comparison to the dynamical processes (>>10 nmol mol^{-1}) observed in the anvil outflow region. The major part of the probed thunderstorms over the central U.S. developed over regions with low mixing ratios of anthropogenic O_3 precursors in the BL, which is assumed to cause the lack of pronounced O_3 production signatures. Rather low O_3 enhancements (<10 nmol mol^{-1}) and production signatures ($\Delta O_3/CO = +0.03$ to $+0.14$) were observed in less undiluted BB and anthropogenic plumes lofted to the LT-MT (~1–7 km) altitude in the vicinity, but outside of the investigated thunderstorms. Occasionally, these pollution plumes (elevated in Θ_e) were even lofted to the UT (~7–10 km) both inside and outside of the thunderstorms and frequently mixed with stratospheric intrusions wrapped around the anvil outflow ($\Delta O_3/CO = -1.7$ to $+1.4$). Even more pronounced $\Delta O_3/CO$ ratios (between -3.9 and $+1.4$) were observed higher up in the anvil outflow region (~9–12 km), due to a stronger and more direct exchange of air masses between the LT and UT/LS region.

In summary, DC3 thunderstorms over the central U.S. seem to act as huge cooking pots, mixing a cocktail of polluted BL air (here especially enhanced in CO from wildfires) with O_3-rich lower stratospheric air and emitting this mixture (together with high amounts of LNO_x) over a surprisingly wide area in the UT/LS region and on a surprisingly regular basis during DC3. We would expect that this aged thunderstorm outflow may have a large impact on the UT/LS composition in general and may contribute to the recurring UT-O_3 maximum observed in a stationary anticyclone centered over the southeastern U.S. in summer by *Li et al*. [2005]. In addition, the aged thunderstorm outflow may impact the UT/LS composition downwind of the U.S. (e.g., North Atlantic), as already observed by, e.g., *Brunner et al*. [1998] and *Jeker et al*. [2000]. Besides the wide horizontal spreading of the thunderstorm outflow during DC3, the frequent development of overshooting cloud tops was also striking. In these cases a large-scale multiple-tropopause structure was present, which may facilitate the development of overshooting tops [*Homeyer et al*., 2014].

It is expected that the impact of thunderstorms on the NO_x and O_3 composition in the UT/LS region will increase in the near future as a response to climate change. Especially within the perspective of increasing global temperatures, frequency of severe thunderstorms and wildfire activity [*Simmonds et al*., 2005; *Brooks*, 2013; *Turetsky et al*., 2011; *Romps et al*., 2014], we recommend further combined, high-resolved model studies, airborne in situ and lidar measurements in the UT/LS region, and ground-based radar measurements on this important topic. The analyses presented here and in HH2016 show that the frequent occurrence of deep and severe convection over the central U.S. is a preferred target region for these kinds of studies. The impact of smoke aerosols on the intensification of central U.S. thunderstorms also needs to be addressed in more detail in future studies.

Acknowledgments
The DC3 field campaign was established by a collaborative effort of NCAR, NASA, the U.S. university community, NOAA, and DLR. The National Science Foundation (NSF), NASA, NOAA, and DLR were the primary funders for DC3. NCAR is supported by the NSF. Detailed information on the scientific goals and a link to the field data is available from the DC3 web site, https://www.eol.ucar.edu/field_projects/dc3. We greatly acknowledge the excellent collaboration with the DC3 principal investigators and all the support the DLR team received during the field phase from M. C. Barth (NCAR), C. A. Cantrell (University of Colorado), W. H. Brune (The Pennsylvania State University), S. A. Rutledge (Colorado State University), and J. H. Crawford (NASA/LaRC). Furthermore, the logistical support from NCAR-EOL by V. Salazar, J. Moore, G. Stossmeister, and B. Baeuerle is greatly appreciated. We thank the Falcon pilots (R. Welser and P. Weber), A. Hausold for the logistics, the engineers, and scientists of the DLR flight department for the excellent support during the field phase. We express our gratitude to the DLR colleagues who supported the trace gas and aerosol measurements: U. Schumann, J. Kim, A. Reiter, A. Roiger, H. Ziereis, and the financial support from the Deutsche Forschungsgemeinschaft (DFG, project number MI 583/4-1). Furthermore, the ETH Zurich (T. Peters) is greatly acknowledged for providing the NO instrument, J. Brioude (NOAA) for providing FLEXPART model products, and S. Kondragunta (NOAA/NESDIS) for providing GOME-2 NO_2 retrieval products. The GOES data were provided by NCAR/EOL under sponsorship of the National Science Foundation (http://data.eol.ucar.edu/). We thank L. L. Pan and C. R. Homeyer (NCAR Boulder) for fruitful discussions. Finally, we are grateful to A. Roiger (DLR) and the three anonymous reviewers for their helpful comments and suggestions, which greatly helped to improve the manuscript.

References

Allen, D. J., K. E. Pickering, R. W. Pinder, B. H. Henderson, K. W. Appel, and A. Prados (2012), Impact of lightning-NO on eastern United States photochemistry during the summer of 2006 as determined using the CMAQ model, *Atmos. Chem. Phys.*, *12*, 1737–1758, doi:10.5194/acp-12-1737-2012.

Allen, D., K. E. Pickering, B. Duncan, and M. Damon (2010), Impact of lightning NO emissions on North American photochemistry as determined using the Global Modeling Initiative (GMI) model, *J. Geophys. Res.*, *115*, D22301, doi:10.1029/2010JD014062.

Alvarado, M. J., et al. (2010), Nitrogen oxides and PAN in plumes from boreal fires during ARCTAS-B and their impact on ozone: An integrated analysis of aircraft and satellite observations, *Atmos. Chem. Phys.*, *10*, 9739–9760, doi:10.5194/acp-10-9739-2010.

Anderson, J. G., D. M. Wilmouth, J. B. Smith, and D. S. Sayres (2012), UV dosage levels in summer: Increased risk of ozone loss from convectively injected water vapor, *Science*, *337*, 835, doi:10.1126/science.1222978.

Apel, E. C., et al. (2012), Impact of the deep convection of isoprene and other reactive trace species on radicals and ozone in the upper troposphere, *Atmos. Chem. Phys.*, *12*, 1135–1150, doi:10.5194/acp-12-1135-2012.

Apel, E. C., et al. (2015), Upper tropospheric ozone production from lightning NO_x-impacted convection: Smoke ingestion case study from the DC3 campaign, *J. Geophys. Res. Atmos.*, *120*, 2505–2523, doi:10.1002/2014JD022121.

Barth, M. C., J. Lee, A. Hodzic, G. Pfister, W. C. Skamarock, J. Worden, J. Wong, and D. Noone (2012), Thunderstorms and upper troposphere chemistry during the early stages of the 2006 North American Monsoon, *Atmos. Chem. Phys.*, *12*, 11,003–11,026, doi:10.5194/acp-12-11003-2012.

Barth, M. C., et al. (2015), The Deep Convective Clouds and Chemistry (DC3) Field Campaign, *Bull. Am. Meteorol. Soc.*, *96*, 1281–1309, doi:10.1175/BAMS-D-13-00290.1.

Bertschi, I. T., and D. A. Jaffe (2005), Long-range transport of ozone, carbon monoxide, and aerosols to the NE Pacific troposphere during the summer of 2003: Observations of smoke plumes from Asian boreal fires, *J. Geophys. Res.*, *110*, D05303, doi:10.1029/2004JD005135.

Biggerstaff, M. I., and R. A. Houze Jr. (1993), Kinematics and microphysics of the transition zone of the 10–11 June, 1985 squall-line system, *J. Atmos. Sci.*, *50*, 3091–3110, doi:10.1175/1520-0469[1993)050<3091:KAMOTT>2.0.CO;2.

Biggerstaff, M. I., L. J. Wicker, J. Guynes, C. L. Ziegler, J. M. Straka, E. N. Rasmussen, A. Doggett, L. D. Carey, J. L. Schroeder, and C. Weiss (2005), The Shared Mobile Atmospheric Research and Teaching radar: A collaboration to enhance research and teaching, *Bull. Am. Meteorol. Soc.*, *86*, 1263–1274, doi:10.1175/BAMS-86-9-1263.

Blyth, A. M., W. A. Cooper, and J. B. Jensen (1988), A study of the source of entrained air in Montana cumuli, *J. Atmos. Sci.*, *45*, 3944–3964, doi:10.1175/1520-0469[1988)045<3944:ASOTSO>2.0.CO;2.

Boatman, J. F., and A. H. Auer (1983), The role of cloud top entrainment in cumulus clouds, *J. Atmos. Sci.*, *40*, 1517–1534, doi:10.1175/1520-0469[1983)040<1517:TROCTE>2.0.CO;2.

Bolton, D. (1980), The computation of equivalent potential temperature, *Mon. Weather Rev.*, *108*, 1046–1053, doi:10.1175/1520-0493[1980)108<1046:TCOEPT>2.0.CO;2.

Bozem, H., et al. (2014), Influence of corona discharge on the ozone budget in the tropical free troposphere: A case study of deep convection during GABRIEL, *Atmos. Chem. Phys. Discuss.*, *14*, 5233–5270, doi:10.5194/acpd-14-5233-2014.

Brooks, H. E. (2013), Severe thunderstorms and climate change, *Atmos. Res.*, *123*, 129–138, doi:10.1016/j.atmosres.2012.04.002.

Brunner, D., J. Staehelin, and D. Jeker (1998), Large-scale nitrogen oxide plumes in the tropopause region and implications for ozone, *Science*, *282*, 1305–1309, doi:10.1126/science.282.5392.1305.

Bucsela, E., E. Celarier, M. Wenig, J. F. Gleason, P. Veefkind, K. F. Boersma, and E. Brinksma (2006), Algorithm for NO_2 vertical column retrieval from the Ozone Monitoring Instrument, *IEEE Trans. Geosci. Remote Sens.*, *44*, 1245–1258, doi:10.1109/TGRS.2005.863715.

Chin, M., D. J. Jacob, J. W. Munger, D. D. Parrish, and B. G. Doddridge (1994), Relationship of ozone and carbon monoxide over North America and its implication for ozone production and transport, *J. Geophys. Res.*, *99*, 14,565–14,573, doi:10.1029/94JD00907.

Choi, Y., Y. Wang, T. Zeng, R. V. Martin, T. P. Kurosu, and K. Chance (2005), Evidence of lightning NOx and convective transport of pollutants in satellite observations over North America, *Geophys. Res. Lett.*, *32*, L02805, doi:10.1029/2004GL021436.

Choi, Y., Y. Wang, T. Zeng, D. Cunnold, E. Yang, R. Martin, K. Chance, V. Thouret, and E. Edgerton (2008), Springtime transitions of NO_2, CO, and O_3 over North America: Model evaluation and analysis, *J. Geophys. Res.*, *113*, D20311, doi:10.1029/2007JD009632.

Cooper, O. R., et al. (2006), Large upper tropospheric ozone enhancements above midlatitude North America during summer: In situ evidence from the IONS and MOZAIC ozone measurement network, *J. Geophys. Res.*, *111*, D24S05, doi:10.1029/2006JD007306.

Cooper, O. R., et al. (2007), Evidence for a recurring eastern North America upper tropospheric ozone maximum during summer, *J. Geophys. Res.*, *112*, D23304, doi:10.1029/2007JD008710.

Cooper, O. R., et al. (2009), Summertime buildup and decay of lightning NO_x and aged thunderstorm outflow above North America, *J. Geophys. Res.*, *114*, D01101, doi:10.1029/2008JD010293.

Cooper, O., et al. (2004), A case study of trans-Pacific warm conveyor belt transport: The influence of merging airstreams on trace gas import to North America, *J. Geophys. Res.*, *109*, D23S08, doi:10.1029/2003JD003624.

Crutzen, P. J. (1970), The influence of nitrogen oxides on the atmospheric ozone content, *Q. J. R. Meteorol. Soc.*, *96*, 320–325, doi:10.1002/qj.49709640815.

Crutzen, P. J. (1995), Overview of tropospheric chemistry: Developments during the past quarter century and a look ahead, in *Faraday Discussions on Atmospheric Chemistry—Measurements, Mechanics and Models*, vol. 100, pp. 1–21, Royal Society of Chemistry, Cambridge, doi:10.1039/FD9950000001.

Cummins, K. L., and M. J. Murphy (2009), An overview of lightning locating systems: History, techniques, and data uses, with an in-depth look at the U.S. NLDN, *IEEE Trans. Electromagn. Compat.*, *51*(3), 499–518.

de Reus, M., J. Ström, P. Hoor, J. Lelieveld, and C. Schiller (1999), Particle production in the lowermost stratosphere by convective lifting of the tropopause, *J. Geophys. Res.*, *104*, 23,935–23,940, doi:10.1029/1999JD900774.

DeCaria, A. J., K. E. Pickering, G. L. Stenchikov, and L. E. Ott (2005), Lightning-generated NOx and its impact on tropospheric ozone production: A three-dimensional modeling study of a Stratosphere–Troposphere Experiment: Radiation, Aerosols and Ozone (STERAO-A) thunderstorm, *J. Geophys. Res.*, *110*, D14303, doi:10.1029/2004JD005556.

Dickerson, R. R., et al. (1987), Thunderstorms: An important mechanism in the transport of air pollutants, *Science*, *235*, 460–465, doi:10.1126/science.235.4787.460.

Draxler, R. R., and Rolph, G. D. (2014), HYSPLIT (HYbrid Single-Particle Lagrangian Integrated Trajectory) Model, access via NOAA ARL READY Website (http://ready.arl.noaa.gov/HYSPLIT.php), NOAA Air Resources Laboratory, Silver Spring, Md.

Dye, J. E., et al. (2000), An overview of the Stratospheric-Tropospheric Experiment: Radiation, Aerosols, and Ozone (STERAO)-Deep Convection experiment with results for the July 10, 1996 storm, *J. Geophys. Res.*, *105*(D8), 10,023–10,045, doi:10.1029/1999JD901116.

Fischer, H., et al. (2003), Deep convective injection of boundary layer air into the lowermost stratosphere at midlatitudes, *Atmos. Chem. Phys.*, *3*, 739–745, doi:10.5194/acp-3-739-2003.

Fishman, J., and W. Seiler (1983), Correlative nature of ozone and carbon monoxide in the troposphere: Implications for the tropospheric ozone budget, *J. Geophys. Res.*, *88*, 3662–3670, doi:10.1029/JC088iC06p03662.

Fishman, J., S. Solomon, and P. J. Crutzen (1979), Observational and theoretical evidence in support of a significant in situ photochemical source of tropospheric ozone, *Tellus*, *31*, 432–446, doi:10.1111/j.2153-3490.1979.tb00922.x.

Folkins, I., C. Braun, A. M. Thompson, and J. Witte (2002), Tropical ozone as an indicator of deep convection, *J. Geophys. Res.*, *107*(D13), 4184, doi:10.1029/2001JD001178.

Frey, W., R. Schofield, P. Hoor, D. Kunkel, F. Ravegnani, A. Ulanovsky, S. Viciani, F. D'Amato, and T. P. Lane (2015), The impact of overshooting deep convection on local transport and mixing in the tropical upper troposphere/lower stratosphere (UTLS), *Atmos. Chem. Phys. Discuss.*, *15*, 1041–1091, doi:10.5194/acpd-15-1041-2015.

Hecobian, A., et al. (2011), Comparison of chemical characteristics of 495 biomass burning plumes intercepted by the NASA DC-8 aircraft during the ARCTAS/CARB-2008 field campaign, *Atmos. Chem. Phys.*, *11*, 13,325–13,337, doi:10.5194/acp-11-13325-2011.

Hegglin, M. I., et al. (2004), Tracing troposphere-to-stratosphere transport above a mid-latitude deep convective system, *Atmos. Chem. Phys.*, *4*, 741–756, doi:10.5194/acp-4-741-2004.

Hitchman, M. H., M. L. Buker, G. J. Tripoli, R. B. Pierce, J. A. Al-Saadi, E. V. Browell, and M. A. Avery (2004), A modeling study of an East Asian convective complex during March 2001, *J. Geophys. Res.*, *109*, D15S14, doi:10.1029/2003JD004312.

Homeyer, C. R., K. P. Bowman, L. L. Pan, M. A. Zondlo, and J. F. Bresch (2011), Convective injection into stratospheric intrusions, *J. Geophys. Res.*, *116*, D23304, doi:10.1029/2011JD016724.

Homeyer, C. R., L. L. Pan, and M. C. Barth (2014), Transport from convective overshooting of the extratropical tropopause and the role of large-scale lower stratosphere stability, *J. Geophys. Res. Atmos.*, *119*, 2220–2240, doi:10.1002/2013JD020931.

Houze, R. A. (2004), Mesoscale convective systems, *Rev. Geophys.*, *42*, RG4003, doi:10.1029/2004RG000150.

Houze, R. A., Jr., S. A. Rutledge, M. I. Biggerstaff, and B. F. Smull (1989), Interpretation of Doppler weather radar displays in midlatitude mesoscale convective systems, *Bull. Am. Meteorol. Soc.*, *70*, 608–619, doi:10.1175/1520-0477[1989)0702.0.CO;2.

Hudman, R. C., L. T. Murray, D. J. Jacob, S. Turquety, S. Wu, D. B. Millet, M. Avery, A. H. Goldstein, and J. Holloway (2009), North American influence on tropospheric ozone and the effects of recent emission reductions: Constraints from ICARTT observations, *J. Geophys. Res.*, *114*, D07302, doi:10.1029/2008JD010126.

Huntrieser, H., H. Schlager, C. Feigl, and H. Höller (1998), Transport and production of NO_x in electrified thunderstorms: Survey of previous studies and new observations at mid-latitudes, *J. Geophys. Res.*, *103*, 28,247–28,264, doi:10.1029/98JD02353.

Huntrieser, H., et al. (2002), Airborne measurements of NO_x, tracer species and small particles during the European Lightning Nitrogen Oxides Experiment, *J. Geophys. Res.*, *107*(D11), 4113, doi:10.1029/2000JD000209.

Huntrieser, H., H. Schlager, A. Roiger, M. Lichtenstern, U. Schumann, C. Kurz, D. Brunner, C. Schwierz, A. Richter, and A. Stohl (2007), Lightning-produced NO_x over Brazil during TROCCINOX: Airborne measurements in tropical and subtropical thunderstorms and the importance of mesoscale convective systems, *Atmos. Chem. Phys.*, *7*, 2987–3013, doi:10.5194/acp-7-2987-2007.

Huntrieser, H., U. Schumann, H. Schlager, H. Höller, A. Giez, H.-D. Betz, D. Brunner, C. Forster, O. Pinto Jr., and R. Calheiros (2008), Lightning activity in Brazilian thunderstorms during TROCCINOX: Implications for NO_x production, *Atmos. Chem. Phys.*, *8*, 921–953, doi:10.5194/acp-8-921-2008.

Huntrieser, H., et al. (2009), NO_x production by lightning in Hector: First airborne measurements during SCOUT-O3/ACTIVE, *Atmos. Chem. Phys.*, *9*, 8377–8412, doi:10.5194/acp-9-8377-2009.

Huntrieser, H., H. Schlager, M. Lichtenstern, P. Stock, T. Hamburger, H. Höller, K. Schmidt, H.-D. Betz, A. Ulanovsky, and F. Ravegnani (2011), Mesoscale convective systems observed during AMMA and their impact on the NO_x and O_3 budget over West Africa, *Atmos. Chem. Phys.*, *11*, 2503–2536, doi:10.5194/acp-11-2503-2011.

Huntrieser, H., et al. (2016), Injection of lightning-produced NO_x, water vapor, wildfire emissions, and stratospheric air to the UT/LS as observed from DC3 measurements, *J. Geophys. Res. Atmos.*, doi:10.1002/2015JD024273.

Jaffe, D. A., and N. L. Wigder (2012), Ozone production from wildfires: A critical review, *Atmos. Environ.*, *51*, 1–10, doi:10.1016/j.atmosenv.2011.11.063.

Jeker, D. P., L. Pfister, A. M. Thompson, D. Brunner, K. E. Pickering, D. J. Boccippio, H. Wernli, Y. Kondo, and J. Staehelin (2000), Measurements of nitrogen oxides at the tropopause—Attributions to convection and correlation with lightning, *J. Geophys. Res.*, *105*, 3679–3700, doi:10.1029/1999JD901053.

Jourdain, L., S. S. Kulawik, H. M. Worden, K. E. Pickering, J. Worden, and A. M. Thompson (2010), Lightning NO_x emissions over the USA constrained by TES ozone observations and the GEOS-Chem model, *Atmos. Chem. Phys.*, *10*, 107–119, doi:10.5194/acp-10-107-2010.

Kley, D., P. J. Crutzen, H. G. J. Smit, H. Vömel, S. J. Oltmans, H. Grassl, and V. Ramanathan (1996), Observations of near-zero ozone concentrations over the convective Pacific: Effects on air chemistry, *Science*, *274*, 230–233, doi:10.1126/science.274.5285.230.

Lemon, L. R., and C. A. Doswell III (1979), Severe thunderstorm evolution and meso-cyclone structure as related to tornadogenesis, *Mon. Weather Rev.*, *107*, 1184–1197, doi:10.1175/1520-0493[1979)107<1184:STEAMS>2.0.CO;2.

Li, Q., D. J. Jacob, R. Park, Y. Wang, C. L. Heald, and R. Hudman (2005), North American pollution outflow and the trapping of convectively lifted pollution by upper-level anticyclone, *J. Geophys. Res.*, *110*, D10301, doi:10.1029/2004JD005039.

Liang, Q., et al. (2007), Summertime influence of Asian pollution in the free troposphere over North America, *J. Geophys. Res.*, *112*, D12S11, doi:10.1029/2006JD007919.

Maddox, R. A. (1980), Mesoscale convective complexes, *Bull. Am. Meteorol. Soc.*, *61*, 1374–1387, doi:10.1175/1520-0477[1980)061<1374:MCC>2.0.CO;2.

Morris, G. A., A. M. Thompson, K. E. Pickering, S. Chen, E. J. Bucsela, and P. A. Kucera (2010), Observations of ozone production in a dissipating tropical convective cell during TC4, *Atmos. Chem. Phys.*, *10*, 11,189–11,208, doi:10.5194/acp-10-11189-2010.

Mullendore, G. L., D. R. Durran, and J. R. Holton (2005), Cross-tropopause tracer transport in midlatitude convection, *J. Geophys. Res.*, *110*, D06113, doi:10.1029/2004JD005059.

Myhre, G., et al. (2013), Anthropogenic and natural radiative forcing, in *Climate Change 2013: The Physical Science Basis. Contribution of Working Group I to the Fifth Assessment Report of the Intergovernmental Panel on Climate Change*, edited by T. F. Stocker et al., pp. 659–740, Cambridge Univ. Press, Cambridge, U. K., and New York, doi:10.1017/CBO9781107415324.018.

Nowak, J. B., et al. (2004), Gas-phase chemical characteristics of Asian emission plumes observed during ITCT 2 K2 over the eastern North Pacific Ocean, *J. Geophys. Res.*, *109*, D23S19, doi:10.1029/2003JD004488.

Ott, L. E., K. E. Pickering, G. L. Stenchikov, H. Huntrieser, and U. Schumann (2007), Effects of lightning NO_x production during the July 21 European Lightning Nitrogen Oxides Project storm studied with a three-dimensional cloud-scale chemical transport model, *J. Geophys. Res.*, *112*, D05307, doi:10.1029/2006JD007365.

Pan, L. L., et al. (2014), Thunderstorms enhance tropospheric ozone by wrapping and shedding stratospheric air, *Geophys. Res. Lett.*, *41*, 7785–7790, doi:10.1002/2014GL061921.

Parrish, D. D., J. S. Holloway, M. Trainer, P. C. Murphy, F. L. Forbes, and F. C. Fehsenfeld (1993), Export of North American pollution ozone to the North Atlantic Ocean, *Science*, *259*, 1436–1439, doi:10.1126/science.259.5100.1436.

Parrish, D. D., J. S. Holoway, R. Jakoubek, M. Trainer, T. B. Ryerson, G. Hübler, F. C. Fehsenfeld, J. L. Moody, and O. R. Cooper (2000), Mixing of anthropogenic pollution with stratospheric ozone: A case study from the North Atlantic wintertime troposphere, *J. Geophys. Res.*, *105*, 24,363–24,374, doi:10.1029/2000JD900291.

Payne, C. D., T. J. Schuur, D. R. MacGorman, M. I. Biggerstaff, K. M. Kuhlman, and W. D. Rust (2010), Polarimetric and electrical characteristics of a lightning ring in a supercell storm, *Mon. Weather Rev.*, *138*, 2405–2425, doi:10.1175/2009MWR3210.1.

Pfister, G. G., L. K. Emmons, J. F. Hess, A. M. Thompson, and J. E. Yorks (2008), Analysis of the summer 2004 ozone budget over the United States using Intercontinental Transport Experiment Ozonesonde Network Study (IONS) observations and Model of Ozone and Related Tracers (MOZART-4) simulations, *J. Geophys. Res.*, *113*, D23306, doi:10.1029/2008JD010190.

Pickering, K. E., A. M. Thompson, R. R. Dickerson, W. T. Luke, D. P. McNamara, J. P. Greenberg, and P. R. Zimmerman (1990), Model calculations of tropospheric ozone production potential following observed convective events, *J. Geophys. Res.*, *95*, 14,049–14,062, doi:10.1029/JD095iD09p14049.

Pickering, K. E., et al. (1996), Convective transport of biomass burning emissions over Brazil during TRACE A, *J. Geophys. Res.*, *101*, 23,993–24,012, doi:10.1029/96JD00346.

Potvin, C. K., D. Betten, L. J. Wicker, K. L. Elmore, and M. I. Biggerstaff (2012), 3DVAR versus traditional dual-Doppler wind retrievals of a simulated supercell thunderstorm, *Mon. Weather Rev.*, *140*, 3487–3494, doi:10.1175/MWR-D-12-00063.1.

Poulida, O., R. R. Dickerson, and A. Heymsfield (1996), Stratosphere-troposphere exchange in a midlatitude mesoscale convective complex. Part 1: Observations, *J. Geophys. Res.*, *101*, 6823–6836, doi:10.1029/95JD03523.

Price, H. U., D. A. Jaffe, O. R. Cooper, and P. V. Doskey (2004), Photochemistry, ozone production, and dilution during long-range transport episodes from Eurasia to the northwest United States, *J. Geophys. Res.*, *109*, D23S13, doi:10.1029/2003JD004400.

Ray, E. A., et al. (2004), Evidence of the effect of summertime midlatitude convection on the subtropical lower stratosphere from CRYSTAL-FACE tracer measurements, *J. Geophys. Res.*, *109*, D18304, doi:10.1029/2004JD004655.

Real, E., et al. (2010), Cross-hemispheric transport of central African biomass burning pollutants: Implications for downwind ozone production, *Atmos. Chem. Phys.*, *10*, 3027–3046, doi:10.5194/acp-10-3027-2010.

Ridley, B. A., M. A. Avery, J. V. Plant, S. A. Vay, D. D. Montzka, A. J. Weinheimer, D. J. Knapp, J. E. Dye, and E. C. Richard (2006), Sampling of chemical constituents in electrically active convective systems: Results and cautions, *J. Atmos. Chem.*, *54*, 1–20, doi:10.1007/s10874-005-9007-5.

Roach, W. T. (1967), On the nature of the summit areas of severe storms in Oklahoma, *Q. J. R. Meteorol. Soc.*, *93*, 318–336, doi:10.1002/qj.49709339704.

Rolph, G. D. (2014), Real-time Environmental Applications and Display sYstem (READY), Website (http://ready.arl.noaa.gov), NOAA Air Resources Laboratory, Silver Spring, Md.

Romps, D. M., J. T. Seeley, D. Vollaro, and J. Molinari (2014), Projected increase in lightning strikes in the United States due to global warming, *Science*, *346*, 851–854, doi:10.1126/science.1259100.

Schroeder, J. R., L. L. Pan, T. Ryerson, G. Diskin, J. Hair, S. Meinardi, I. Simpson, B. Barletta, N. Blake, and D. R. Blake (2014), Evidence of mixing between polluted convective outflow and stratospheric air in the upper troposphere during DC3, *J. Geophys. Res. Atmos*, *119*, 11,477–11,491, doi:10.1002/jgrd.v119.19.

Schumann, U., and H. Huntrieser (2007), The global lightning-induced nitrogen oxides source, *Atmos. Chem. Phys.*, *7*, 3823–3907, doi:10.5194/acp-7-3823-2007.

Simmonds, P. G., A. J. Manning, R. G. Derwent, P. Ciais, M. Ramonet, V. Kazan, and D. Ryall (2005), A burning question. Can recent growth rate anomalies in the greenhouse gases be attributed to large-scale biomass burning events?, *Atmos. Environ.*, *39*, doi:10.1016/j.atmosenv.2005.02.018.

Singh, H. B., et al. (2010), Pollution influences on atmospheric composition and chemistry at high northern latitudes: Boreal and California forest fire emissions, *Atmos. Environ.*, *44*, 4553–4564, doi:10.1016/j.atmosenv.2010.08.026.

Stenchikov, G., R. Dickerson, K. Pickering, W. Ellis Jr., B. Doddridge, S. Kondragunta, O. Poulida, J. Scala, and W.-K. Tao (1996), Stratosphere-troposphere exchange in a mid-latitude mesoscale convective complex: Part 2, numerical simulations, *J. Geophys. Res.*, *101*, 6837–6851, doi:10.1029/95JD02468.

Stevenson, D. S., et al. (2006), Multimodel ensemble simulations of present-day and near-future tropospheric ozone, *J. Geophys. Res.*, *111*, D08301, doi:10.1029/2005JD006338.

Stohl, A., C. Forster, S. Eckhardt, N. Spichtinger, H. Huntrieser, J. Heland, H. Schlager, S. Wilhelm, F. Arnold, and O. Cooper (2003), A backward modeling study of intercontinental pollution transport using aircraft measurements, *J. Geophys. Res.*, *108*(D12), 4370, doi:10.1029/2002JD002862.

Suhre, K., J.-P. Cammas, P. Nedelec, R. Rosset, A. Marenco, and H. G. J. Smit (1997), Ozone-rich transients in the upper equatorial Atlantic troposphere, *Nature*, *388*, 661–663, doi:10.1038/41749.

Tang, Q., and M. J. Prather (2010), Correlating tropospheric column ozone with tropopause folds: The Aura-OMI satellite data, *Atmos. Chem. Phys.*, *10*, 9681–9688, doi:10.5194/acp-10-9681-2010.

Tang, Q., M. J. Prather, and J. Hsu (2011), Stratosphere-troposphere exchange ozone flux related to deep convection, *Geophys. Res. Lett.*, *38*, L03806, doi:10.1029/2010GL046039.

Thompson, A. M., W. K. Tao, K. E. Pickering, J. R. Scala, and J. Simpson (1997), Tropical deep convection and ozone formation, *Bull. Am. Meteorol. Soc.*, *78*, 1043–1054, doi:10.1029/95JD03523.

Thornton, D. C., A. R. Bandy, B. W. Blomquist, J. D. Bradshaw, and D. R. Blake (1997), Vertical transport of sulfur dioxide and dimethyl sulfide in deep convection and its role in new particle formation, *J. Geophys. Res.*, *102*, 28,501–28,510, doi:10.1029/97JD01647.

Turetsky, M. R., E. S. Kane, J. W. Harden, R. D. Ottman, K. L. Maines, E. Hoy, and E. S. Kashschke (2011), Recent acceleration of biomass burning and carbon losses in Alaskan forests and peatlands, *Nat. Geosci.*, *4*, 27–31, doi:10.1038/NGEO1027.

Wang, C., P. J. Crutzen, V. Ramanathan, and S. F. Williams (1995), The role of a deep convective storm over the tropical Pacific Ocean in the redistribution of atmospheric chemical species, *J. Geophys. Res.*, *100*, 11,509–11,516, doi:10.1029/95JD01173.

Wang, L., M. J. Newchurch, A. Pour-Biazar, S. Kuang, M. Khan, X. Liu, W. Koshak, and K. Chance (2013), Estimating the influence of lightning on upper tropospheric ozone using NLDN lightning data and CMAQ model, *Atmos. Environ.*, *67*, 219–228, doi:10.1016/j.atmosenv.2012.11.001.

Wang, P. K. (2003), Moisture plumes above thunderstorm anvils and their contributions to cross-tropopause transport of water vapor in midlatitudes, *J. Geophys. Res.*, *108*(D6), 4194, doi:10.1029/2002JD002581.

Wang, Y., S. C. Liu, B. E. Anderson, Y. Kondo, G. L. Gregory, G. W. Sachse, S. A. Vay, D. R. Blake, H. B. Singh, and A. M. Thompson (2000), Evidence of convection as a major source of condensation nuclei in the northern midlatitude upper troposphere, *Geophys. Res. Lett.*, *27*, 369–372, doi:10.1029/1999GL010930.

Wigder, N. L., and D. A. Jaffe (2013), Ozone and particulate matter enhancements from regional wildfires observed at Mount Bachelor during 2004–2011, *Atmos. Environ.*, *75*, 24–31, doi:10.1016/j.atmosenv.2013.04.026.

Winterrath, T., T. P. Kurosu, A. Richter, and J. P. Burrows (1999), Enhanced O_3 and NO_2 in thunderstorm clouds: Convection or production? *Geophys. Res. Lett.*, *26*, 1291–1294, doi:10.1029/1999GL900243.

Yang, Q., et al. (2015), Aerosol transport and wet scavenging in deep convective clouds: A case study and model evaluation using a multiple passive tracer analysis approach, *J. Geophys. Res. Atmos.*, *120*, 8448–8468, doi:10.1002/2015JD023647.

Zahn, A., C. A. M. Brenninkmeijer, P. J. Crutzen, D. D. Parrish, D. Sueper, G. Heinrich, H. Güsten, H. Fischer, M. Hermann, and J. Heintzenberg (2002), Electrical discharge source for tropospheric "ozone-rich transients", *J. Geophys. Res.*, *107*(D22), 4638, doi:10.1029/2002JD002345.

Zhao, C., Y. Wang, Y. Choi, and T. Zeng (2009), Summertime impact of convective transport and lightning NO_x production over North America: Modeling dependence on meteorological simulations, *Atmos. Chem. Phys.*, *9*, 4315–4327, doi:10.5194/acp-9-4315-2009.